APPLICATION OF WALL FUNCTIONS TO LARGE EDDY SIMULATIONS FOR CHANNEL FLOW AT LOW AND HIGH REYNOLDS NUMBERS

DÜŞÜK VE YÜKSEK REYNOLDS SAYILARINDA KANALDAKİ BİR AKIŞTA DUVAR FONKSİYONLARININ LARGE EDDY SİMÜLASYONUNA UYGULANMASI

UFUK KORKMAZ

Submitted to
HACETTEPE UNIVERSITY
THE INSTITUTE OF GRADUATE STUDIES
IN SCIENCE AND ENGINEERING
in partial fulfillment of the requirements for the degree of
MASTER OF SCIENCE
in
NUCLEAR ENGINEERING

2010

APPLICATION OF WALL FUNCTIONS TO LARGE EDDY SIMULATIONS FOR A CHANNEL FLOW AT LOW AND HIGH REYNOLDS NUMBERS

Ufuk Korkmaz

ABSTRACT

Turbulent flow in a channel geometry for low and high friction Reynolds numbers and turbulent heat transfer at a high Reynolds number were analyzed by Large-Eddy Simulation (LES). LES was performed with the application of the wall functions. Influence of two subgrid scale (SGS) models, the Smagorinsky and Vreman models along with the model constant parameters on numerical results were investigated. Sensitivity of the obtained results with respect to spatial discretization in the streamwise and spanwise directions was examined. Simulations with various distances of the first computational mesh points to the wall were performed to test the application of wall functions. LES results obtained with the OpenFoam open-source computational code were compared with available high-resolution direct numerical simulations (DNS). Additionally, direct numerical simulations were performed using OpenFoam for low Reynolds number to check the accuracy of the numerical schemes.Turbulent heat transfer was examined for constant wall heat flux and temperature boundary conditions to test the implementation of the thermal wall functions for various distances from the wall.

From the influence of subgrid scale constant, LES Smagorinsky simulations gave better results when the Smagorinsky constant was particularly adjusted for a channel flow. Whereas the Vreman model gave much better results without being influenced by the value of the Smagorinsky constant. It was found from the investigations of the influence of SGS model, the subgrid scale eddy-viscosity model had no significant influence on the LES results. It was found for turbulent heat transfer part, SGS model had large influence on the mean temperature profile. Similarly, wall functions had an impact on the mean and root mean square (rms) fluctuations.

Keywords: channel flow, LES, subgrid scale model, wall functions, OpenFoam, Smagorinsky model, Vreman model, turbulent heat transfer

Supervisor: Assoc. Prof. Dr. C. Niyazi Sökmen, Hacettepe University, Department of Nuclear Engineering

Co-supervisor: Dr. Arkadiusz K. Kuczaj, Nuclear Research and Consultancy Group (NRG), Safety and Performance Group

DÜŞÜK VE YÜKSEK REYNOLDS SAYILARINDA KANALDAKİ BİR AKIŞTA DUVAR FONKSİYONLARININ LARGE EDDY SİMÜLASYONUNA UYGULANMASI

Ufuk Korkmaz

ÖZ

Bu çalışma bir kanalda türbülanslı akışın düşük ve yüksek sürtünme Reynolds sayılarında incelenmesini içermektedir. Ayrıca, türbülanslı ısı transferi bu akış için yüksek Reynolds sayısında incelenmiştir. Bu çalışmadaki bütün simülasyonlar Büyük Girdap Simülasyonu (LES) ile duvar fonksiyonları kullanarak gerçekleştirilmiştir. Alt grid ölçek modellerinden biri olan Smagorinsky ve Vreman modellerinin ve model sabitlerinin Büyük Girdap Simülasyonu (LES) sonuçları üzerindeki etkisi incelenmiştir. Akış ve derinlik yönlerinde kullanılan sayısal ağ sıklığının sonuçlar üzerindeki etkisine bakılmıştır. Duvar fonksiyonlarının uygulanışının test edilmesi için değişen duvar uzaklıkları için simülasyonlar yapılmıştır. OpenFoam ile elde edilen Büyük Girdap Simülasyonu (LES) sonuçlarıyla, deneme problemi DNS verileri karşılaştırılmıştır. Düşük Reynolds sayısında OpenFoam ile OpenFoam'un nümerik şemasını test etmek için Doğrudan Nümerik Simülasyon (DNS) gerçekleştirilmiştir. Türbülanslı ısı transferi sabit duvar ısı akısı ve sabit sıcaklık sınır koşulları gibi iki ayrı durumda incelenmiştir. Buradaki amaç termal duvar fonksiyonlarının duvardan değişik uzaklıklarda bu koşullar için uygulanmasının test edilmesidir.

Alt ölçek model sabitinin etkilerinin test edildiği simülasyonlar sonucunda, Smagorinsky modeli simülasyonunun sonuçlarının model sabitinin kanalda akış için uygun bir değere getirildikten sonra daha iyi bir sonuç verdiği gözlenmiştir. Buna karşılık Vreman modelinin model sabitinden bağımsız olarak çok daha iyi sonuçlar verdiği anlaşılmıştır. Alt ölçek modellerinin etkilerinin test edildiği simülasyonlarda alt ölçek girdap viskos modelinin sonuçlar üzerinde kayda değer bir etkisi olmadığı görülmüştür. Türbülanslı ısı transferi kısmında, alt grid ölçek modelinin ortalama sıcaklık profili üzerinde büyük etkisinin olduğu görülmüştür. Aynı şekilde duvar fonksiyonlarının ortalama ve ortalama kare kök hızlarının üzerinde etkili olduğu ortaya çıkmıştır.

Anahtar Kelimeler: kanal akışı, Büyük Girdap Simülasyonu, alt grid ölçek modeli, duvar fonksiyonları, OpenFoam, Smagorinsky modeli, Vreman modeli, türbülanslı ısı transferi

Danışman: Doç. Dr. C. Niyazi Sökmen, Hacettepe Üniversitesi, Nükleer Enerji Mühendisliği Bölümü

Eş Danışman: Dr. Arkadiusz K. Kuczaj, Nükleer Araştırma ve Danışmanlık Grubu (NRG), Güvenlik ve Performans Bölümü

ACKNOWLEDGMENT

I would like to express my gratitude to all those who gave me the possibility to complete this thesis. First, I want to thank my professors from the Department of Nuclear Engineering for encouraging and allowing me to complete this thesis at the Nuclear Research and Consultancy Group (NRG) in the Netherlands. I would like to thank to my supervisor **Assoc. Prof. C. Niyazi Sökmen** for his support, guidance and encouragement. I also want to thank my co-supervisor **Arek Kuczaj** from whom I learned a lot about turbulence. I am grateful to him for his patience, support and help throughout the thesis.

My colleagues from NRG supported me in my work during nine months. I want to thank to all of them for their help and friendships. I am grateful to NRG for give me the opportunity to complete my master thesis at NRG.

Also, I would like to thank **Hüseyin and Belgin Özdemir** from Netherlands. I am thankful to them for their help. It would be very difficult for me living abroad without their support.

Special thanks goes to **Atilla Yıldız** who shared, understood all of my feelings and supported me with his love during nine months away from my country.

The last but not least, I would like to give the best thanks to my wonderful **family**, who stand by me in my difficult times. I owe them all success I have in my life and I want to dedicate this thesis to them.

TABLE OF CONTENTS

LIST OF FIGURES

Page

LIST OF TABLES

Page

NOMENCLATURE

LES	: Large-Eddy Simulation
k	: Wave Number
E	: Kinetic Energy
$\langle\varepsilon\rangle$	: Mean Dissipation Rate
ν	: Viscosity
η	: Kolmogorov Scale
υ	: Kolmogorov Velocity Scale
τ	: Kolmogorov Time Scale
DNS	: Direct Numerical Simulation
RANS	: Reynolds Averaged Navier-Stokes
$\overline{u}$	: Resolved Velocity
u'	: Subgrid Scale Velocity
$\overline{u_i}$	: Filtered Velocity
G	: Filter Function
Δ	: Filter Width
D	: Computational Domain
SGS	: Subgrid Scale
τ_{ij}	: Subgrid Scale Stress
ν_t	: Eddy-viscosity
$\lvert\overline{S}\rvert$	: Magnitude of Stress Rate Tensor
C_s	: Smagorinsky Constant
y^+	: The distance to the nearest wall represented in the wall units
u_τ	: Friction Velocity
A^+	: A constant used in Van Driest damping function
u^+	: Dimensionless Velocity
κ	: Von Karman constant
δ	: Channel half-width
x	: Streamwise Direction
y	: Wall-normal Direction
z	: Spanwise Direction
N_x	: Number of Grid Points in x-direction
N_y	: Number of Grid Points in y-direction
N_z	: Number of Grid Points in z-direction
Δx^+	: Grid Size in x-direction in the non-dimensional units
Δz^+	: Grid Size in z-direction in the non-dimensional units
g_H	: Growing Factor
Re_τ	: Friction Reynolds Number
Re_m	: Reynolds number based on bulk mean velocity
Pr	: Prandtl Number
μ	: Dynamic Viscosity
ρ	: Density
α	: Thermal Diffusivity
c_p	: Specific Heat Capacity

$\bar{T}$	: Filtered Temperature
q_w	: Wall-heat Flux
U_c	: Mean Centerline Velocity
u, v, w	: Velocity Components
$\bar{T}_p$	: Periodic part of the temperature
$\bar{T}_m$	: Linear Part of the temperature
t	: Time
T_τ	: Friction Temperature
∇T	: Temperature Gradient
T^+	: Non-dimensional Temperature
$\alpha_{\texttt{eff}}$	: Effective-diffusivity
rms	: Root Mean Square (The root-mean-square of a variate x is
	: the square root of the mean squared value of x: $R(x) \equiv \sqrt{\langle x^2 \rangle}$)
T_w	: Wall Temperature
CFD	: Computational Fluid Dynamics

1 INTRODUCTION

This chapter is devoted to the introduction of the main terms used in examination of the turbulent channel flow with Large-Eddy Simulations (LES). Particular attention was paid to present the governing equations. Details concerning turbulent heat transfer, case geometry and reference cases will be presented here. The aim and outline of the thesis are also mentioned in this section.

1.1 Turbulence Scales

Turbulent flows are often characterized by a presence of various scales of motion. The size of the largest scales of the fluid motion (often called eddies) are usually dictated by the overall geometry of the examined flow. Historically, turbulence was characterized by a cascade of such eddies, in which the biggest eddies of the size of the flow geometry break up into smaller eddies and this process is continued until they are sufficiently small to be dissipated by viscous forces. Such description represents the *cascading process* defined by Richardson [1]. The cascading process is shown in the Fig. 1.1.

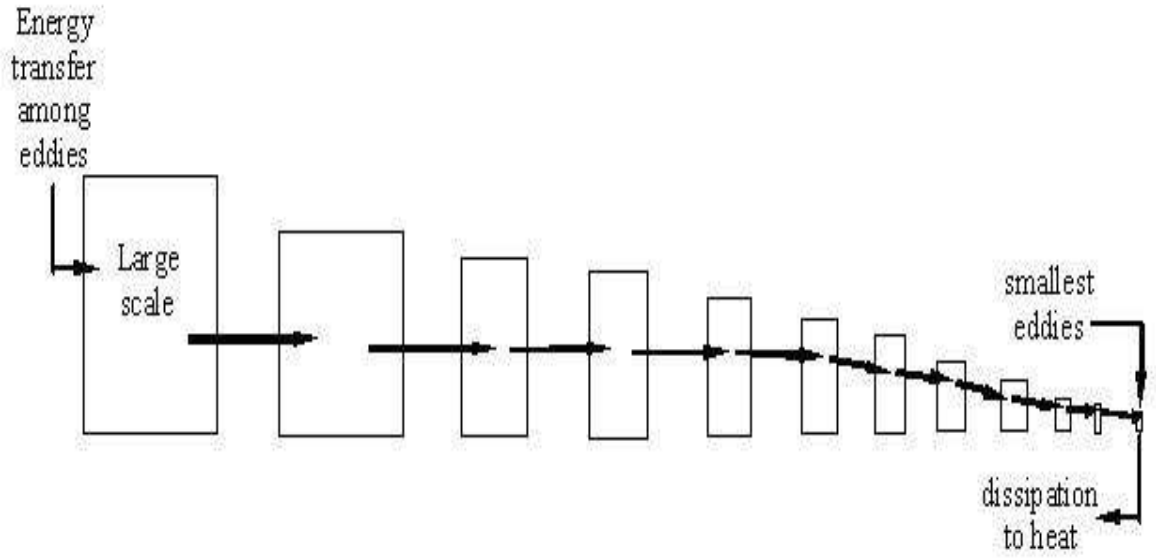

FIGURE 1.1: *Schematic sketch of the energy cascading process.*

In general, most of the flows seen in nature and laboratory conditions are non

homogeneous and anisotropic. Kolmogorov postulated that during the cascade process geometrical and directional information contained in a turbulent flow is gradually lost and the smallest scales are homogeneous and isotropic [1]. Despite the mean flow and large-scale eddies, he assumed that there is a range of scales where the flow is locally homogeneous and isotropic. In this region the flow description for sufficiently small scales and sufficiently high Reynolds number should be universal. Independent from of the type of flow it is determined by only two parameters. These are the mean dissipation rate $\langle\varepsilon\rangle$ [m^2/s^3], and viscosity ν [m^2/s]. The dissipation rate is the rate at which the turbulence energy is converted to the thermal energy by viscous effects. Using dimensional analysis, we may show that the smallest scale where the viscosity plays an important role is given by $\eta = \left(\nu^3/\langle\varepsilon\rangle\right)^{1/4}$ [m] (often called Kolmogorov scale). The Kolmogorov velocity scale υ [m/s] and time scale τ [s] are given by $\upsilon = \left(\nu\langle\varepsilon\rangle\right)^{1/4}$, and $\tau = \left(\nu/\varepsilon\right)^{1/2}$. His second hypothesis assumes that the universal regime description extends to scales, which are much larger than η but much smaller than the integral length scale that is usually dictated by the eddies that contain most of the energy in the flow. In this region, the flow is determined by the average dissipation rate $\langle\varepsilon\rangle$. The Kolmogorov's description of turbulence works well for many experiments. The kinetic energy in spectral space is usually presented by plotting the amplitudes of Fourier components (E) versus wave numbers (k) associated with the entire spectral range, i.e., from the large scales where turbulence is produced to the smallest where the energy is dissipated. A typical energy spectrum is shown in the Fig. 1.2. The Kolmogorov's description assumes that the kinetic energy is transported from the large scales to small scales via the intermediate scales present in the so-called inertial range. In this region, energy is neither produced nor dissipated, but it is handed down to smaller and smaller scales. This is known as the turbulence energy cascade. The turbulent scales are independent both of the large scales and the small scales if the Reynolds number is large. This region is characterized by ε and wave number k. Thus the energy of an eddy in this region can be estimated as $E(k) \sim \varepsilon^{2/3}k^{-5/3}$. This expression is called *Kolmogorov Spectrum Law* or *-5/3 power law*.

In order to obtain accurate numerical solution of the Navier-Stokes equations, all scales present in a flow must be computed on the computational mesh with a proper

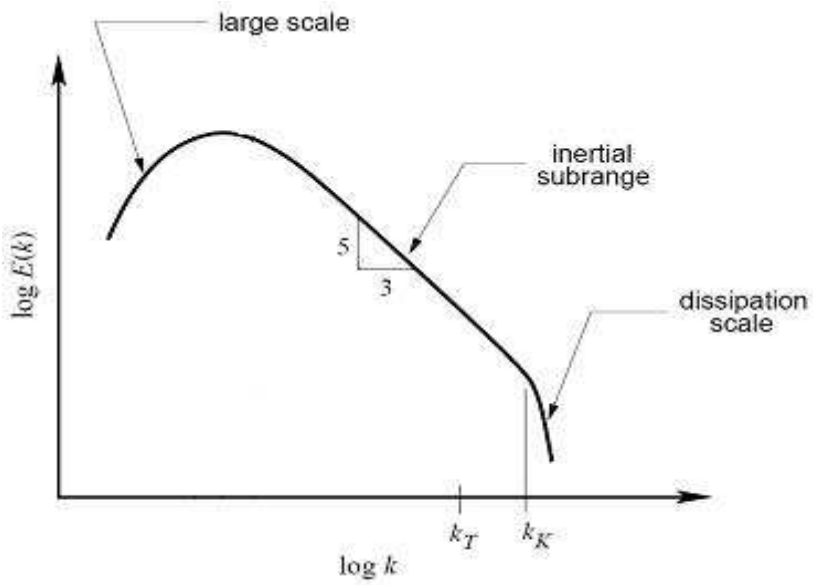

FIGURE 1.2: *Typical energy spectrum observed in a turbulent flow.*

resolution. All the spatial and temporal scales of turbulence must be resolved during such simulations. This approach is known as the Direct Numerical Simulations (DNS). Such an approach is very expensive from the computational point of view and it is not possible for most of the practical applications. To overcome this issue a modeling technique was developed, which is known as Large-Eddy Simulations (LES). As suggested by the name, LES resolves only large scales present in a flow. Smaller scales are accounted by application of a model. This can be schematically represented using the energy spectrum plot. Three different regions of the spectrum are shown in Fig. 1.3. Region I is associated with the large scales, which are directly resolved on the computational grid. Region II represents a hypothetical inertial range, in which an LES model can be applied to account for a proper dissipation of energy, which mainly takes place in region III. This will be explained in more detail in the following section of the thesis. Another numerical approach, which computes only the mean flow is the Reynolds Averaged Navier-Stokes (RANS) modeling technique [2]. In this case, all scales present in a flow are accounted by a model. While RANS methods provide averaged results, LES is able to predict instantaneous flow characteristics and resolve turbulent flow structures. LES also offers significantly more accurate results over RANS.

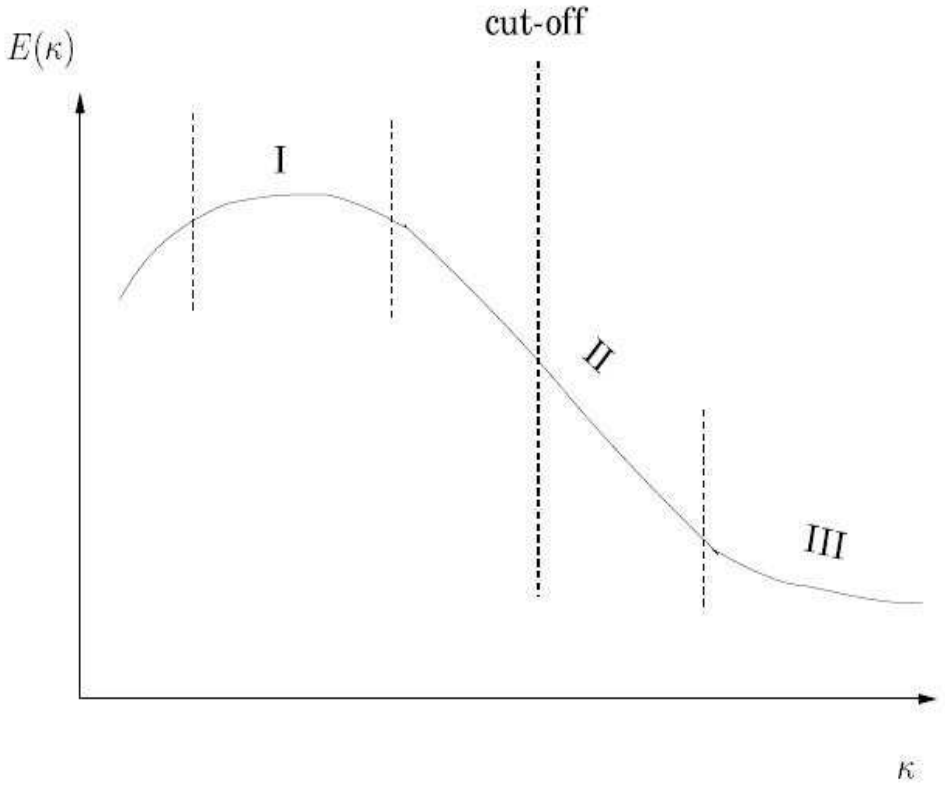

FIGURE 1.3: *Schematic sketch of the energy spectrum divided into three different regions .(I-, II-, III-)*

1.2 Large-Eddy Simulation (LES)

A general idea standing behind Large-Eddy Simulations is to compute large scales present in a turbulent flow while using a model for smaller ones that cannot be resolved on the computational mesh [3]. This follows an assumption that large eddies, which contain most of energy, determine the main flow dynamics. The small eddies are only responsible for dissipation of the kinetic energy. It is assumed that they are homogeneous/isotropic and they can be modeled using for example an eddy-viscosity assumption. In order to separate the small scales from the large scales, a filtering operation is applied to the Navier-Stokes equations. The velocity field $\mathbf{u}$ is decomposed into a sum of the resolved scales $\overline{\mathbf{u}}$ and the subgrid scale contribution $\mathbf{u}$'. Filtering operation is applied to the Navier-Stokes equations: $\overline{\mathbf{u}} = \int_D G(\varsigma, \Delta)\mathbf{u}(\varsigma, t)d^3\varsigma$, where G is the filter function, Δ is the characteristic scale of the filter function (filter-width), and D is the computational domain. As a result of this operation a filtered version of the Navier-Stokes equations is obtained together

with the incompressibility condition. These equations are written below in the index notation form:

$$\frac{\partial \overline{u_i}}{\partial t} + \frac{\partial \left(\overline{u_i}\,\overline{u_j}\right)}{\partial x_j} + \frac{1}{\rho}\frac{\partial \overline{p}}{\partial x_i} - \nu\frac{\partial^2 \overline{u_i}}{\partial x_j \partial x_j} = -\frac{\partial \tau_{ij}}{\partial x_j}, \tag{1.1}$$

$$\frac{\partial \overline{u_i}}{\partial x_i} = 0. \tag{1.2}$$

Since $\overline{u_i u_j} \neq \overline{u_i}\,\overline{u_j}$, the filtered form of the equations is usually rewritten to the form in which the subgrid scale (SGS) tensor, τ_{ij} is introduced:

$$\tau_{ij} = \overline{u_i u_j} - \overline{u_i}\,\overline{u_j} \tag{1.3}$$

This term needs to be modeled in LES and it will be briefly described in the next section, where the already mentioned eddy-viscosity concept will be presented.

1.2.1 Subgrid-Scale modeling

Due to application of the filtering procedure to the Navier-Stokes equations, the corresponding filtered equations must be closed by an appropriate subgrid-scale model. The most commonly used subgrid-scale models in engineering applications are based on an *eddy-viscosity* assumption. In this case, an additional viscosity is introduced to the Navier-Stokes equations, which accounts for a dissipative character of small scales. The Smagorinsky SGS model is a typical example of the eddy-viscosity model. In this model, the subgrid scale tensor is defined as:

$$\tau_{ij} = -2\nu_t \overline{S_{ij}} + \frac{1}{3}\delta_{ij}\tau_{kk}, \tag{1.4}$$

where ν_t is the eddy viscosity and $\overline{S_{ij}}$ is the strain rate tensor. The strain rate tensor is defined as:

$$\overline{S_{ij}} = \frac{1}{2}\left(\frac{\partial \overline{u_i}}{\partial x_j} + \frac{\partial \overline{u_j}}{\partial x_i}\right). \tag{1.5}$$

The eddy-viscosity has the following formulation:

$$\nu_t = (C_s \Delta)^2 \left|\overline{S}\right|, \tag{1.6}$$

where Δ is the filter width, $\left|\overline{S}\right|$ is the magnitude of the strain rate tensor and it is defined as:

$$\left|\overline{S}\right| = \sqrt{2\overline{S}_{ij}\overline{S}_{ij}}. \tag{1.7}$$

The Smagorinsky model has many advantages as for example its simplicity, but in general it must be tuned for the practical flows via the so-called Smagorinsky constant C_s, which is present in this model. The value of C_s may vary from 0.065 recommended for a channel flow to 0.2 for the isotropic turbulence [4]. Furthermore, the Smagorinsky model produces large amount of dissipation near the wall, which has to be reduced. Usually, the so-called damping functions are used in order to obtain correct distribution of viscosity in the near wall region. Often the Van Driest damping function is used, which modifies the Smagorinsky constant near the wall:

$$C_s = C_{s0}\left(1 - e^{-y^+/A^+}\right)^2 \tag{1.8}$$

where y^+ is a distance to the nearest wall represented in the wall units:

$$y^+ = \frac{yu_\tau}{\nu}. \tag{1.9}$$

In this expression, $u_\tau = (\tau_w/\rho)^{1/2}$ $[m/s]$ is the friction velocity, where τ_w is wall shear stress. A^+ is a constant, usually set to 25 and C_{s0} is the Smagorinsky constant in the region away from the boundaries. When y^+ exceeds some typical value, $\exp -y^+$ term is effectively zero. In Fig. 1.4 behavior of the Van Driest damping function near to the wall is plotted for $C_{s0} = 0.065$.

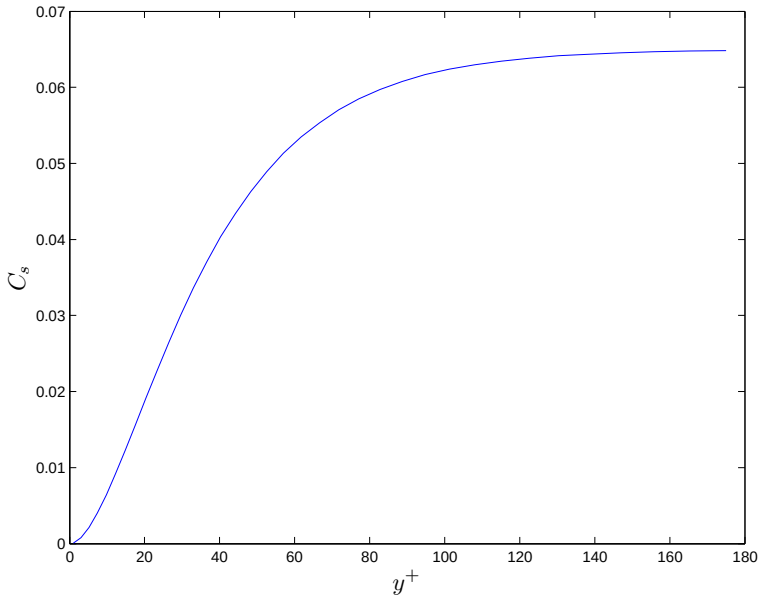

FIGURE 1.4: *Van Driest damping function with* $C_{s0} = 0.065$*.*

The Smagorinsky model predicts non-vanishing subgrid-scale eddy viscosity in the regions where the flow is laminar and the eddy viscosity should be zero.

In the computational setup of this study recently developed Vreman subgrid-scale eddy-viscosity model [5] will be examined. In this model, vanishing subgrid-scale dissipation for the shear flow near to the wall is guaranteed even with a non-zero constant model coefficient. The Vreman model showed that it is able to predict turbulence statistics for a channel flow without introducing additional wall-damping functions. The model provides desirable features for large-eddy simulation and it does not require any averaging or clipping procedures for the numerical stabilization, which is particularly important for complex flow configurations. The subgrid scale eddy viscosity is modeled as:

$$\nu_t = c\sqrt{\frac{\bar{B}_\beta}{\bar{\alpha}_{ij}\bar{\alpha}_{ij}}} \tag{1.10}$$

where

$$\bar{B}_\beta = \bar{\beta}_{11}\bar{\beta}_{22} - \bar{\beta}_{12}\bar{\beta}_{12} + \bar{\beta}_{11}\bar{\beta}_{33} - \bar{\beta}_{13}\bar{\beta}_{13} + \bar{\beta}_{22}\bar{\beta}_{33} - \bar{\beta}_{23}\bar{\beta}_{23}, \tag{1.11}$$

$$\bar{\beta}_{ij} = \sum_{m=1}^{3} \overline{\triangle}_m^2 \bar{\alpha}_{mi}\bar{\alpha}_{mj}, \tag{1.12}$$

$$\overline{\alpha}_{ij} = \frac{\partial \overline{u}_j}{\partial x_i} \tag{1.13}$$

The model constant c is related to the Smagorinsky constant C_s by the following relation $c \approx 2.5C_s^2$. $\overline{\triangle_m}$ is the grid filter width in the '*m*' direction. The symbol α_{ij} represents the (3x3) matrix of derivatives of the filtered velocity $\bar{u}$.

1.2.2 Wall functions

Many flows are usually associated with boundaries at which the most of turbulence is generated. They are usually called the wall bounded shear flows. In such flows, the near wall region needs particular attention. As turbulent structures generated in the near wall region are much smaller than those present in bulk of the flow, computational meshes in this region must be enormously fine to accurately resolve small scale flow features. In most of the practical cases such approach is too expensive for the available computational resources. A quite common approach in LES was borrowed from the RANS simulations, where the wall functions are used. Wall functions provide an explicit formula for the mean turbulent velocity profile near a solid boundary. By applying wall functions in the near wall region, resolving of small flow features in this region at the price of having rather artificial flow conditions

that are bounded to the wall was avoided. Behavior of the velocity near to the wall was examined in detail by appropriate numerical simulations and experiments [2].

The velocity profiles near the wall are usually represented in the non-dimensional wall units, which are connected with the friction velocity (shear stress). It was found that in the region very close to the wall, velocity profile exhibits a linear behavior as viscous effects are dominant in this region. The velocity profile in this region is associated with $u^+ = y^+$, where u^+ is the dimensionless velocity: $u^+ = \frac{u}{u_\tau}$, and y^+ was introduced earlier in Eq. (1.9). Next region close to the viscous layer is called the buffer zone. In this region, the flow is dominated by turbulence coming from bulk of the flow. Hence, it is a transitional region with complicated flow structures that emerge there. Next region, which is dominated by turbulence, is often called the 'log-layer' as the velocity profile in this region can be estimated with the following logarithmic formula:

$$u^+ = \frac{1}{\kappa} \ln y^+ + B. \tag{1.14}$$

There are two parameters in this formula: B and κ (κ is often called the Von Karman constant), which are estimated as 5.5 and 0.40, respectively [6]. A schematic representation of all regions is presented in Fig. 1.5.

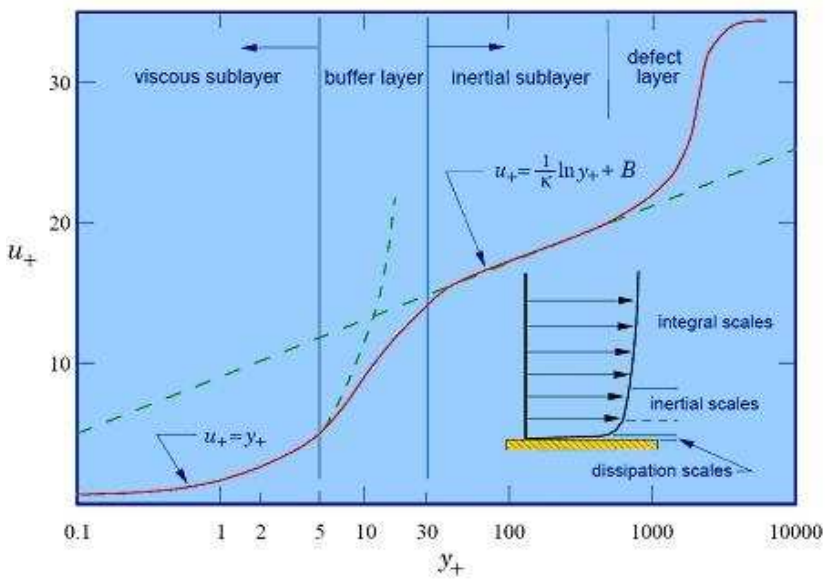

FIGURE 1.5: *Velocity profile for a wall bounded flow presented in the wall units.*

In our simulations, we will test application of wall functions for a particular case of wall bounded flow in a channel, which is described in the next chapters.

1.3 Turbulent Heat Transfer

In this section the turbulent heat transfer in a channel flow is described. Particular attention was paid to the implementation of the thermal wall functions and modeling of the wall heat flux boundary conditions. Main terms related with turbulent heat transfer are described here.

Incorporation of the heat transfer in the incompressible NS equations involves implementation of additional components in the OpenFoam source code:

- passive scalar temperature equation attached to the Navier Stokes equations,
- periodic boundary conditions for the temperature in the streamwise direction and the constant wall heat flux boundary conditions at the walls,
- the Jayatilleke thermal wall functions for LES.

1.3.1 Passive scalar temperature equation

To calculate the turbulent heat fluxes the eddy diffusivity is determined. Similarly as for the Navier-Stokes equations, the eddy-diffusivity concept is used in the modeling of the temperature (energy) equations. In this case, for the incompressible flow, the passive scalar equation is introduced. A passive scalar does not affect the dynamics of the fluid, but it is driven by the convection:

$$\frac{\partial \bar{T}}{\partial t} + u_j \frac{\partial \bar{T}}{\partial x_j} = \frac{\partial}{\partial x_i}(\alpha + \alpha_t \frac{\partial \bar{T}}{\partial x_i}), \tag{1.15}$$

where $\alpha = \frac{\lambda}{\rho c_p}$ $[m^2/s]$ is the thermal diffusivity (the ratio of thermal conductivity to volumetric heat capacity), λ is the thermal conductivity $[W/(m \cdot K)]$, ρ is density $[kg/m^3]$, c_p is specific heat capacity $[J/(kg \cdot K)]$, $\alpha_t = \nu_t / Pr_t$ is the eddy diffusivity, where Pr_t is the turbulent Prandtl number and ν_t $[m^2/s]$ is the SGS eddy-viscosity. The turbulent Prandtl number is the ratio between the momentum eddy diffusivity and the heat transfer eddy diffusivity. From experimental data, Pr_t has an average value of 0.85 in water or air and it may considerably depend on the Prandtl number (Pr) of the fluid, which is set to 0.71. When Pr is small, the heat diffuses very quickly compared to the velocity (momentum) as the thickness of the thermal boundary

TABLE 1.1: *Physical properties used in simulations.*

c_p	4184	$J/kg/K$
ρ	970	kg/m^3
ν	10^{-6}	m^2/s
α	$1.408 \cdot 10^{-6}$	m^2/s
q_w	10	W/m^2
Pr	0.71	
Pr_t	0.85	

layer is much larger than the velocity boundary layer. The physical properties used in simulations are presented in Table 1.1.

In case when constant wall heat flux is applied as the boundary condition, the fluid is heated along the channel domain. As a result, the temperature grows within the domain and it has non-uniform distribution. Moreover, the periodic boundary condition can not be applied. In this case to overcome this issue, we split the temperature into the periodic and linearly changing components:

$$\bar{T}(\mathbf{x}, t) = \Big(\frac{d\bar{T}_m(x)}{dx}\Big)x + \bar{T}_p(\mathbf{x}, t). \tag{1.16}$$

Using Eq. 1.16 in Eq. 1.15, we get:

$$\frac{\partial \bar{T}_p}{\partial t} + u_j\frac{\partial \bar{T}_p}{\partial x_j} = \Big(\alpha + \alpha_t\Big)\frac{\partial^2 \bar{T}_p}{\partial x_j \partial x_j} - C \cdot u_1, \tag{1.17}$$

where $C = \frac{d\bar{T}_m}{dx}$ and $\bar{T}_p$ is the periodic part of the temperature. In order to study only the periodic part of the temperature, the linear part is removed by application of the forcing scheme discussed in section 1.3.2.

1.3.2 Periodic boundary conditions for the temperature equation and the constant wall heat flux boundary conditions for walls

Let's consider flat plate flow with a constant heat flux q_w $[W/m^2]$ boundary conditions that supplies the following energy rate to the computational domain:

$$\dot{q} = \int q_w \cdot dS = q_w \cdot L \cdot W, \tag{1.18}$$

where the geometrical dimensions are specified by the length L and width W. The change in the energy is proportional to the change in the temperature as follows:

$$dq = dm \cdot c_p \cdot dT_m. \tag{1.19}$$

If energy rate is considered, then

$$d\dot{q} = \frac{dm}{dt} \cdot c_p \cdot C dx, \tag{1.20}$$

where the temperature satisfies the linear profile in the x-axis direction: $\frac{dT_m}{dx} = C$, and C is a constant value. Integration over the whole plate gives:

$$\int \Big(\frac{d\dot{q}}{dx}\Big) dS = \int \Big(\dot{m} \cdot c_p \cdot C\Big) dS, \tag{1.21}$$

and finally:

$$\dot{q} = \dot{m} \cdot c_p \cdot C \cdot L. \tag{1.22}$$

The above equation can be used along with the Eq. 1.18 to obtain:

$$C = \frac{q_w \cdot W}{\dot{m} \cdot c_p}. \tag{1.23}$$

For the channel flow, the above equation must be modified to encounter heating from the second plate:

$$C = \frac{2q_w \cdot W}{\dot{m} \cdot c_p} \Big[\frac{K}{m}\Big]. \tag{1.24}$$

Our forcing term can be rewritten as:

$$C \cdot u_1 = \frac{2q_w \cdot W}{\frac{d\rho V}{dt} \cdot c_p} \cdot u_1 = \frac{2q_w \cdot W}{\rho \cdot u_b \cdot W \cdot 2\delta \cdot c_p} \cdot u_1. \tag{1.25}$$

After simple re-arrangement of terms, the above equation simplifies to:

$$C \cdot u_1 = \frac{T_\tau u_\tau}{\delta} \frac{u_1}{u_b}, \tag{1.26}$$

where $T_\tau = \frac{q_w}{\rho c_p u_\tau}$. LES simulations are performed with the constant wall-heat flux boundary conditions and the pseudo steady-state and homogeneous conditions along the x-axis are obtained with 'linear' removal of the heat introduced by both walls via the forcing procedure. It must be noted that in case of simulations described in Ref. [7], the forcing term was used with a reverse sign as the Eq. (1.16) was formulated as: $\bar{T}(\mathbf{x}, t) = \frac{d\bar{T}_m(x)}{dx} x - \bar{T}_p(\mathbf{x}, t)$. In this case, the constant temperature conditions are used, which transfer the heat-flux generated by the positive

forcing with constant heat-flux conditions. Heat flux is defined as the rate of the heat transfer per unit area ($J/(m^2 \cdot s) = W/m^2$). The heat flux is determined by Fourier's law which is proportional to the thermal conductivity k and the temperature gradient ∇T:

$$q_w = -k\nabla T = -\alpha\rho c_p \nabla T \tag{1.27}$$

In the implementation of the constant wall heat flux boundary conditions in LES, the gradient of the temperature is modified as:

$$\nabla \bar{T} = -\frac{q_w}{(\alpha + \alpha_t)\rho c_p}, \tag{1.28}$$

where $\alpha = \frac{k}{\rho c_p}$ is the laminar diffusivity and $\alpha_t = \nu_t / Pr_t$ is the eddy-diffusivity introduced by LES. The sum of the laminar and the eddy-diffusivity is defined as the *effective diffusivity* $\alpha_{\texttt{eff}}$:

$$\alpha_{eff} = \alpha + \alpha_t \tag{1.29}$$

1.3.3 Thermal wall functions

The non-dimensional temperature is defined as $T^+ = (T_w - T)/T_\tau$, where the $T_\tau = q_w/(\rho c_p u_\tau)$ is the friction temperature. The wall heat flux is defined as $q_w = \alpha_{\text{eff}} \rho c_p \frac{T_w - T}{\Delta x}$ where Δx is the length through the heat flux and the diffusivity can be computed as $\alpha_{\text{eff}} = \frac{q_w \Delta x}{\rho c_p (T_w - T)}$. We combine this formula with the non-dimensional temperature:

$$T^+ = \frac{T_w - T}{T_\tau} = \frac{\rho c_p (T_w - T)\Delta x u_\tau}{q_w \Delta x} = \frac{u_\tau \Delta x}{\alpha_{\text{eff}}}, \tag{1.30}$$

Finally, the thermal diffusivity is modified in the following equation:

$$\alpha_{\text{eff}} = \frac{u_\tau \Delta x}{T^+} \tag{1.31}$$

according to the T^+ computed from formula given by [8]:

$$T^+ = \begin{cases} Pr y^+ & \text{if } y^+ < 11; \\ Pr_t \left[\ln(E y^+)/\kappa + P\right] & \text{if } y^+ \geq 11. \end{cases} \tag{1.32}$$

$$P = 9.24 \left[\left(\frac{Pr}{Pr_t} \right)^{3/4} - 1 \right] \left[1 + 0.28 \exp(-0.007 Pr/Pr_t) \right], \tag{1.33}$$

where Pr_t is turbulent Prandtl number (0.85), $\kappa = 0.4187$ and $E = 9$. Similarly as for the momentum, for the temperature law of the wall consists of two different parts:

- linear law for the thermal sublayer in the very near wall region
- logarithmic law for the turbulent region where influence of turbulence dominates

The thickness of the thermal sublayer is in general different from the thickness of the (momentum) viscous sublayer, and it depends on the fluid characteristics. For example, the thickness of the thermal sublayer for a high-Prandtl-number fluid is much smaller than its momentum sublayer thickness. For fluids characterized by the low Prandtl numbers (e.g., liquid metals) the thermal boundary layer is much larger than corresponding momentum sublayer thickness.

1.4 Channel Flow

Channel flow is one of the most simple flow configurations in which various flow conditions can be examined. The flow is directed between two parallel plates and driven via application of additional force to keep either mass flow or pressure drop constant. Periodic boundary conditions are usually applied in the other two directions. In the simulation setup prepared in this study, the constant mass flow is maintained. This is obtained by calculating the averaged mass flow rate (velocity) at each time step and consequently adapting the pressure gradient to keep the mass flow constant.

The flow geometry and the coordinate system are presented in Fig. 1.6. The channel half-width is denoted by δ (total width of the channel is $Y = 2\delta$). The streamwise and spanwise lengths are chosen to be $4\pi\delta$ and $2\pi\delta$, with other dimensions (i.e., X, Z) chosen with respect to the examined cases (Reynolds number). Corresponding number of the grid points in x, y, and z directions are denoted as N_x, N_y and N_z, respectively. In order to test application of wall functions, a number of approaches can be applied for the construction of the numerical grid. To remove uncertain influence of numerical errors and LES modeling, the computational meshes

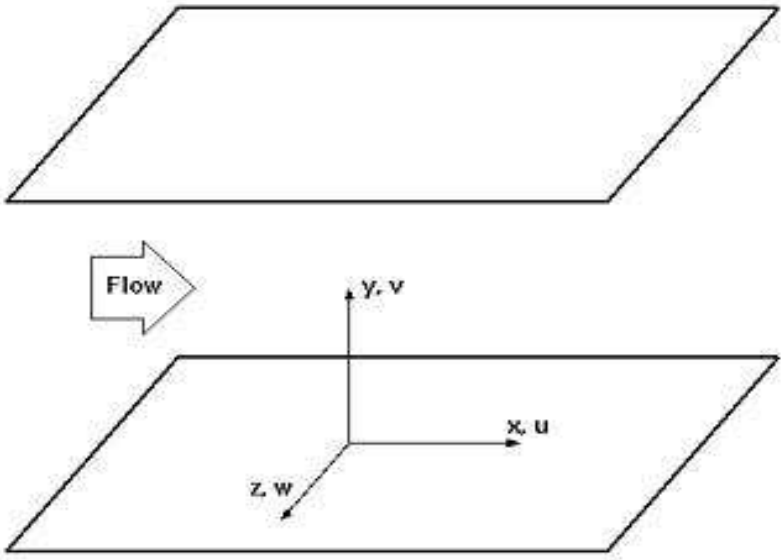

FIGURE 1.6: *Geometry of the channel with coordinate system.*

should be exactly the same apart from the distance of the first computational layer of the grid points next to the wall. Such approach with growing distance from the wall results in a large aspect ratio between two consecutive cell sizes. In the practical applications, the distance from the wall is a limiting factor and usually the consecutive cells are either the same or larger when compared to the first one present next to the wall. This approach allows testing wall functions in more practical setup, but under influence of additional numerical effects that depend on the cell sizes. In this thesis both approaches were followed. For the lower Reynolds number we kept the same constant growing factor in construction (stretching) of the computational mesh in the y-direction starting from the initial wall-distance. The resolution in other two directions was kept the same. As a result, the computational meshes have different sizes. For the larger Reynolds number one numerical mesh with the wall resolved conditions (first computational point at $y^+ < 1$) was constructed. Then, consecutive layers of grid points close to the wall were removed to give meshes that are characterized by various y^+ values and to keep the same cell sizes in the rest of the computational domain. This way similar sizes of the computational meshes were obtained with exactly the same grid structure inside the channel. The channel flow will be investigated for low and high Reynolds conditions. In the Chapter 2 and Chapter 3 of the thesis the flow conditions and computational meshes for the low- and high-Reynolds flows are described in more detail.

TABLE 1.2: *Parameters used for initialization of the flow.*

Δu	$u_b/4$
β^+	$2\pi/200$
α^+	$2\pi/500$
ϵ	$u_b/200$
σ	$5.5 \cdot 10^{-4}$

1.5 Initial Condition

The initial velocity field used in the simulations was obtained from implementation of velocity perturbation. It is used to force transition and reach a fully developed flow sooner. Laminar parabolic velocity profile with imposed perturbations in the spanwise direction is used to initialize the velocity field [9]. The laminar profile is always used as the starting velocity field since an initial turbulent profile damps the perturbations very quickly due to the motion of fluid away from the wall. The laminar profile has the following form:

$$u_{\text{lam}}(y) = u_c\Big(2\frac{y}{\delta} - \Big(\frac{y}{\delta}\Big)^2\Big), \tag{1.34}$$

where u_c is the centerline velocity. The bulk velocity can be computed as:

$$u_b = \frac{1}{2\delta}\int_0^{2\delta} u dy = \frac{2}{3}u_c \tag{1.35}$$

This formulation is equivalent to the velocity profile: $u_{\text{lam}}(y) = u_c\Big(1 - \Big(\frac{y}{\delta}\Big)^2\Big)$ integrated over $[-\delta, \delta]$ domain. The streaks with perturbations are added as:

$$u = u_{\text{lam}} + \frac{\Delta u}{2}\frac{y^+}{30}\exp\Big(-\sigma(y^+)^2 + \frac{1}{2}\Big) \cdot \cos(\beta^+ z^+) \cdot P \tag{1.36}$$

$$w = \epsilon \cdot \sin(\alpha^+ x^+) y^+ \exp\Big(-\sigma(y^+)^2\Big) \cdot P \tag{1.37}$$

where $P = 1 + A \cdot p$ defines the perturbation with the amplitude $A = 0.2$, and p is probability density function for a normal distribution. The other parameters are included in Table 1.2.

1.6 Reference Cases

For the investigation and comparison of the results, the classical channel flow DNS data are taken for the reference purposes. The geometry and flow conditions for those available DNS data for low and high Reynolds number simulations are given in detail in the following section.

1.6.1 Reference case for low Reynolds number simulations

The geometry and conditions used as the reference case for low Reynolds simulations are compliant with the Ercoftac channel flow case No.32 [10]. This database consists of DNS results obtained in channel flow simulations by Kim, Moin and Moser [11]. In these simulations, fully developed turbulent channel flow is numerically investigated. The friction Reynolds number based on the wall shear velocity is $Re_\tau = u_\tau \delta/\nu = 180$. The Reynolds number based on the mean bulk velocity U_m is $Re_m = U_m 2\delta/\nu = 5600$. For this flow Reynolds number based on the mean centerline velocity U_c and the half-channel height is $Re_c = 3300$. The flow is assumed to be homogeneous in the streamwise and spanwise directions. Periodic boundary conditions are used for these directions. The computational domain is chosen to be $4\pi\delta$ and $2\pi\delta$ in the streamwise (x) and spanwise (z) direction. The height of the channel is denoted by 2δ. The computation is carried out with 3962880 computational grid points. The computational domain is discretized with $192 \times 129 \times 160$ points in $x \times y \times z$ directions. The grid sizes in the streamwise and spanwise directions are respectively $\Delta x^+ \approx 12$ and $\Delta z^+ \approx 7$, which are measured in the dimensionless wall units y^+. The non-uniform meshing in the normal direction is used with $y_j = \cos\theta_j$ for $\theta_j = (j-1)\pi/(N_y - 1)$, where $j = 1, 2, \ldots, N_y$ and N_y is the number of grid points in the y-direction. The first computational point from the wall at $\Delta y^+ \approx 1$ corresponds to 0.05 of the physical distance and the maximal spacing (at the centerline of the channel) is 4.4 measured in the dimensionless wall units. Profiles of the mean velocity, root mean square velocities and Reynolds shear stress are non dimensionalized by the wall shear velocity u_τ.

1.6.2 Reference case for high Reynolds number and LES of turbulent heat transfer simulations

The geometry and flow conditions used as the reference case for high Reynolds simulations are based on the DNS simulation [Database of Wall Turbulence and Heat Transfer (Poiseuille channel flow)] performed by Kawamura [12]. The present flow is a fully developed turbulent channel flow driven by a streamwise mean pressure gradient. Periodic condition is imposed in the streamwise and spanwise directions. No-slip boundary condition is applied for the top and bottom walls. The flow is simulated at the friction Reynolds number $Re_\tau = 640$. The Reynolds number based on bulk mean velocity is $Re_m = 24428$. The computational domain is chosen to be $12.8\delta \times 2\delta \times 6.4\delta$ in the streamwise (x), normal (y) and spanwise (z) direction. The height of the channel is denoted by 2δ. The computational domain is discretized with $1024 \times 256 \times 1024$ points in $x \times y \times z$ directions resulting in approximately 268 million grids. The grid sizes in the streamwise and spanwise directions are respectively $\Delta x^+ = 8$ and $\Delta z^+ = 4$, which are measured in the dimensionless wall units y^+.

For turbulent heat transfer case the same flow conditions and geometry are used as in high Reynolds number case. DNS of turbulent heat transfer has been carried out by Kawamura[12] at friction Reynolds number of $Re_\tau = 640$ and Prandtl number of $Pr = \nu/\alpha = 0.71$. The Reynolds number based on the bulk mean velocity is $Re_m = 24428$. The flow is heated with a constant heat flux boundary condition from both walls. Additionally, the temperature fluctuations at the wall are set to zero.

1.7 Aim of the Thesis

The aim of the thesis is to test the application of wall functions applied to LES for channel flow. Channel flow is one of the most classical and simple flow in which various flow conditions can be examined. The flow conditions can be well controlled. The drawback of channel flow is wall-generated turbulence, which makes this test case very demanding with respect to the wall functions. The goal is to check the size of the error introduced by the application of wall functions to LES for different distances from the wall.

Wall functions are developed for Reynolds Averaged Navier-Stokes (RANS) simulations. They are used in the near wall region to avoid from resolving of small turbulent structures. In the thesis, wall functions borrowed from RANS are applied to LES. RANS was not used since it computes only the mean flow. All scales present in a flow are accounted by a model. Contrary to RANS, which provides average results, LES is able to predict instantaneous flow characteristics. As a result, RANS does not supply reliable solutions for fluctuations (rms) in case of turbulent flow. Fluctuations are important for example for thermal fatigue assessments. The drawback of LES is that it needs to have very small meshes particularly close to the wall to resolve the small turbulent structures.

In the thesis, the OpenFoam (Open Field Operation And Manipulation) code is used as a CFD code for simulations. It is an open source code written in C++ for Linux operating systems. The software package consists of pre-configured solvers for specified problems, utilities for pre- and post-processing, and tools for parallel processing [13]. It uses the finite volume method to solve coupled sets of partial differential equations. OpenFOAM offers significant advantages such as users have total freedom to create or modify various solvers.

Information about the general operations of OpenFOAM, input-output data structures, compilation, applications, libraries, mesh generation, post-processing and programming are available in references [13, 14] .

In the thesis, incompressible LES solver called *channelOodles* for channel flow is used to perform the simulations. The *postChannel* utility is used to post-process the data from channel flow calculations. MATLAB is used for the visualization of the data, which are post-processed by *postChannel*.

1.8 Outline of the Thesis

The content of this thesis can be divided into five chapters, including this introduction chapter. In this chapter, important theoretical information about turbulence scales, the governing equations of LES, subgrid scale modeling, wall functions, turbulent heat transfer, the governing equations for temperature, thermal wall functions and brief description of channel flow are introduced.

Chapter 2 deals with channel flow at low Reynolds number. Comparison of obtained DNS and test-case DNS data are presented in Chapter 2. The influence of the two subgrid scale models and model constant on LES results are investigated. The results of LES with the application of wall functions are compared with the available test-case DNS data. Additional simulation results obtained with $k-\epsilon$ turbulence model by using Fluent as CFD code are presented and $k-\epsilon$ model results are compared with LES results in this chapter.

In Chapter 3, the influence of the two subgrid scale models and the spatial discretization are investigated. The LES results are compared with the DNS results. The results obtained by application of wall functions at various wall distances are presented here.

Chapter 4 focuses on LES of turbulent heat transfer. Thermal wall functions are tested for different distances from the wall for constant wall heat flux and wall temperature boundary conditions.

The last chapter summarizes the results and discussions of the thesis and presents final conclusions and suggestions for the future research.

2 CHANNEL FLOW AT LOW REYNOLDS NUMBER

Turbulent flow in a channel geometry is investigated here for low Reynolds number. The main goal of the performed simulations described in this chapter was to obtain appropriate LES flow conditions that must be used in a channel flow. The supplementary direct numerical simulations are presented here. For the investigations, the classical channel flow data (Kim, Moin and Moser) [11] were taken for reference purposes and details were described in Section 1.6.1. The channel flow was simulated at the friction Reynolds number $Re_\tau = 180$. Additionally, the large-eddy simulations are performed here with the application of the wall functions, which are further analyzed in the next chapter.

Turbulent channel flow is a classical test-case in which the numerical schemes and modeling approaches can be efficiently tested in various flow configurations. In this chapter, a flow at low Reynolds number is investigated for which currently direct numerical simulations can be performed with small computational effort. Available DNS data from the high-resolution simulations can be effectively used to test and validate numerical modeling. In this chapter, the following issues are examined:

- comparison of the DNS results for a channel flow obtained by Kim, Moin and Moser with results obtained using OpenFoam,
- study of the LES results with the Smagorinsky subgrid-scale model for various C_s constants and Van Driest damping function,
- study of the LES results obtained with the Vreman subgrid-scale model,
- influence of the eddy-viscosity model on results with comparison to the numerical diffusion introduced by the numerical schemes,
- differences in prediction of rms fluctuations near to the wall with application of meshing with various wall-distance: 1y^+, 2y^+, 4y^+, 8y^+.

The comparison of DNS results obtained using OpenFoam with the reference of Kim,Moin and Moser results was investigated first. OpenFoam DNS simulations are performed with similarly reproduced conditions. The low-Reynolds flow is simulated

at friction Reynolds number of $Re_\tau = u_\tau \delta/\nu = 180$. The bulk mean velocity U_m for $Re_m = U_m 2\delta/\nu = 5600$ is $3.11 \cdot 10^{-4}$m/s. DNS are carried out with 3898368 ($188 \times 128 \times 162$) grid points and 'PISO' (Pressure-Implicit Split-Operator) is used as pressure-velocity coupling method, which is numerical procedure to solve the Navier Stokes equation for transient flow. Time step, Δt is set to 800s. An instantaneous snapshot of the velocity magnitude from these simulations is presented in Fig. 2.1.

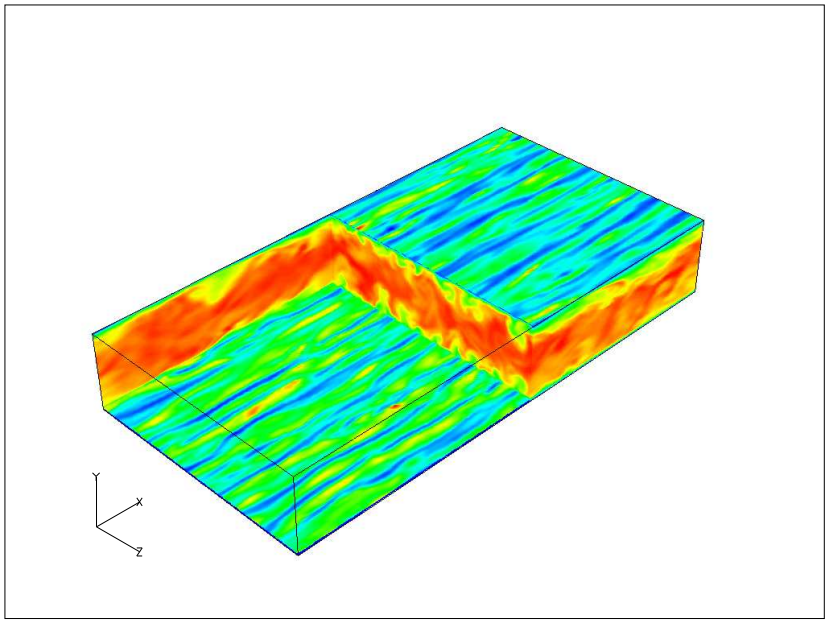

FIGURE 2.1: *Instantaneous snapshot of the velocity magnitude from the OpenFoam DNS simulations.*

2.1 Comparison of DNS Results

In this section the analysis of the results obtained with the OpenFoam DNS simulations that were performed to replicate Kim, Moin and Moser simulations are discussed and accuracy of the OpenFoam numerical schemes is checked. The mean velocity profiles normalized by the wall shear velocity, u_τ equals to $2 \cdot 10^{-5}$m/s are plotted in Fig. 2.2(a). The green dashed line shows the law of the wall, which is analytically represented in the log layer with the following formula: $u^+ = 2.5 \ln y^+ + 5.5$, where 2.5 is the Von Karman constant. In the viscous sublayer, $y^+ < 5$, both DNS result follow the linear law of the wall, which is u^+ equals to y^+. The mean velocity profile obtained with the OpenFoam DNS is very close to those obtained

by Kim, Moin and Moser. The root mean square of velocity components (u, v, w) are shown in Fig. 2.2(b-d). Results obtained with the OpenFoam for all components are slightly under-predicted ($\sim$ 5%) comparing to results obtained by Kim, Moin and Moser. It was verified that the obtained results are reliable in terms of the collected statistics. There are two most likely reasons of this under-prediction. The first one can be connected with a usage of the lower order scheme and the second one can be associated with influence of meshing. Kim, Moin and Moser used a cosine function to stretch the grid, which gives very smooth stretching factor in the buffer region. OpenFoam approach (`blockMesh`) uses the ratio between the first and the last computational cell applying geometric series expansion. These small discrepancies will be not analyzed further in this thesis. All presented comparisons will be made using the obtained results with the OpenFoam package. Further in the text these simulations are referred as 'DNS'.

2.2 Influence of the Smagorinsky Constant

In this section, LES results obtained with two different Smagorinsky constants, i.e., $C_s = 0.13$ and $C_s = 0.065$ are presented. In both cases the Van Driest damping function was used in order to limit the viscous term near to the wall. In addition, simulations with the Vreman model were performed with the same constants as for the Smagorinsky model. The grid sizes in the streamwise and spanwise directions are set $\Delta x^+ \approx 36$ and $\Delta z^+ \approx 21$ for the wall-resolved LES simulations. The same numerical setup and mesh were used in both simulations. In Fig. 2.3(a) the mean velocity profile normalized by the shear velocity, u_τ equals to $2 \cdot 10^{-5}$m/s are presented for simulations with two distinct Smagorinsky constants. As seen from Fig.2.3(a-d), in the buffer and log layers, substantial differences are observed between two simulations performed with different C_s constants. Results with $C_s = 0.13$ are far from the reference DNS results, particularly in the buffer layer. Fig. 2.3(b-d) represent the root mean square (rms) velocity components normalized by the wall shear velocity. We can observe that the peak location of u_{rms} obtained for $C_s = 0.13$ is shifted. The results obtained with the Smagorinsky constant equal 0.065 are over-predicted comparing to the DNS results, but they are much closer that those obtained with

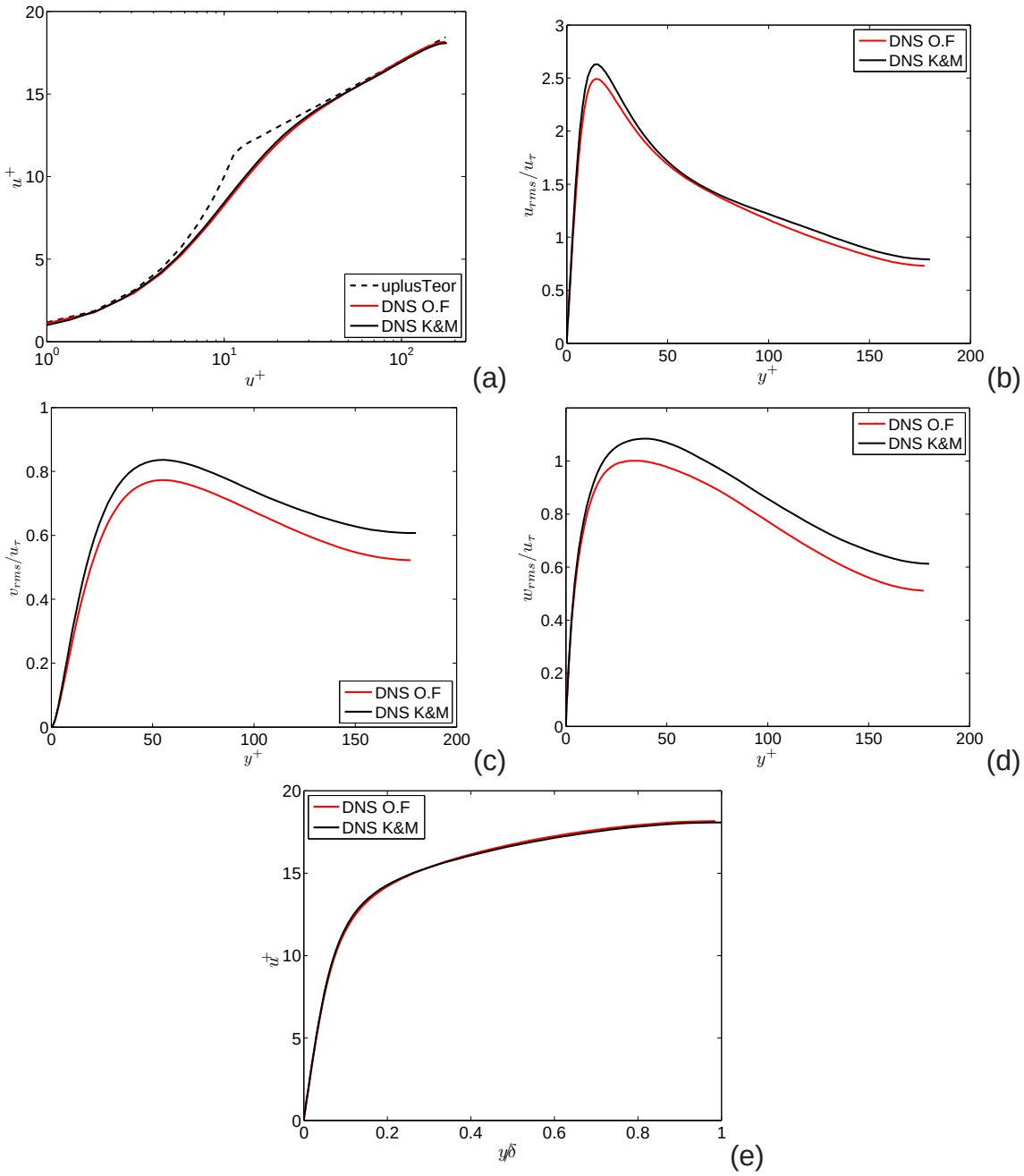

FIGURE 2.2: *Mean velocity profile in wall units (a), in global coordinates (e) and rms velocity fluctuations in three directions (b-d) obtained with DNS. The logarithmic law of the wall denoted by dashed line.*

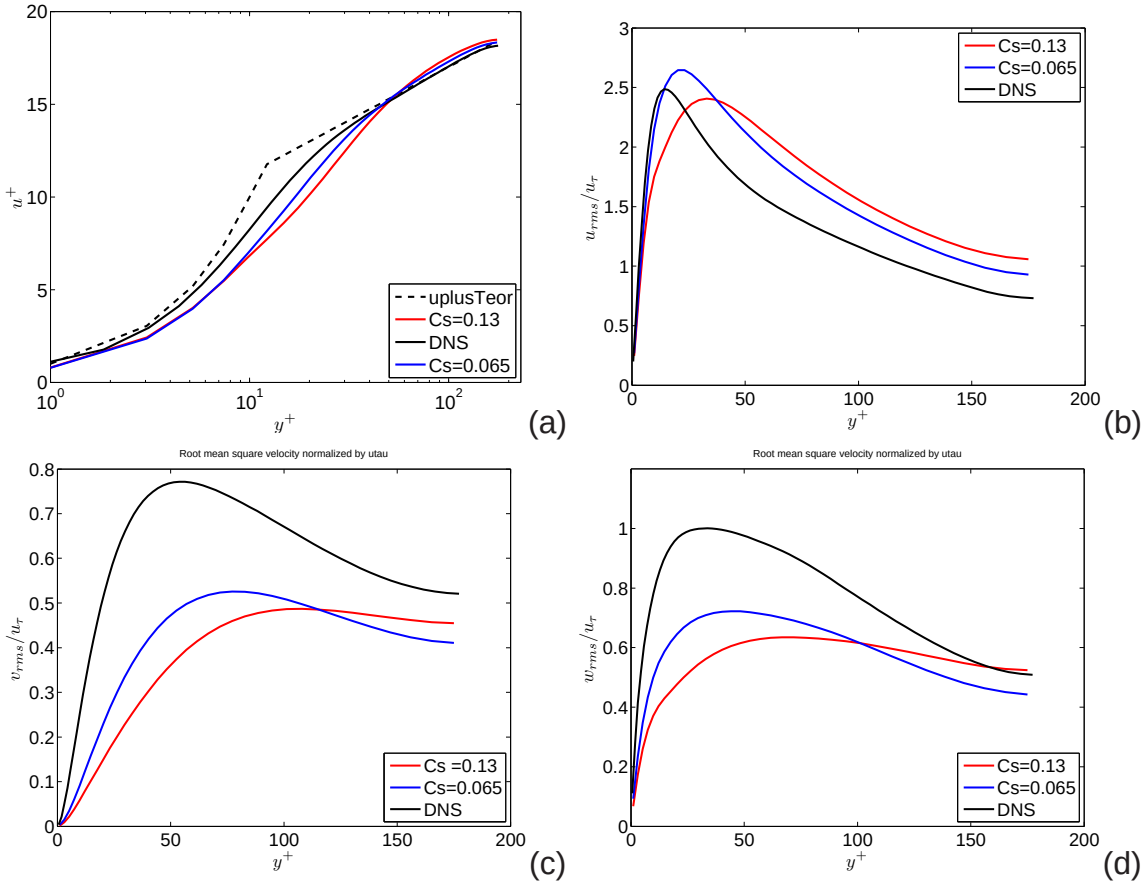

FIGURE 2.3: *Mean velocity profile (a) and rms velocity fluctuations in three directions (b-d) obtained with Smagorinsky with two different Smagorinsky constants.*

$C_s = 0.13$. Difference between LES and DNS results for the rms velocity in x-direction is on average 5%. The peak values for other rms values and shear values are 30% lower compared to the DNS results. Simulations with $C_s = 0.065$ give better results for a channel flow and will be used for further comparisons.

As seen from Fig. 2.4 for all components of the velocity, there is only a small difference between results obtained with the Vreman model computed with two constant values (0.13, 0.065). This suggests a small sensitivity of the model with respect to the modeling parameter.

2.3 SGS Model Strength

In this section, results obtained with two eddy-viscosity subgrid models are compared. These are the Smagorinsky model with the additional Van Driest damping

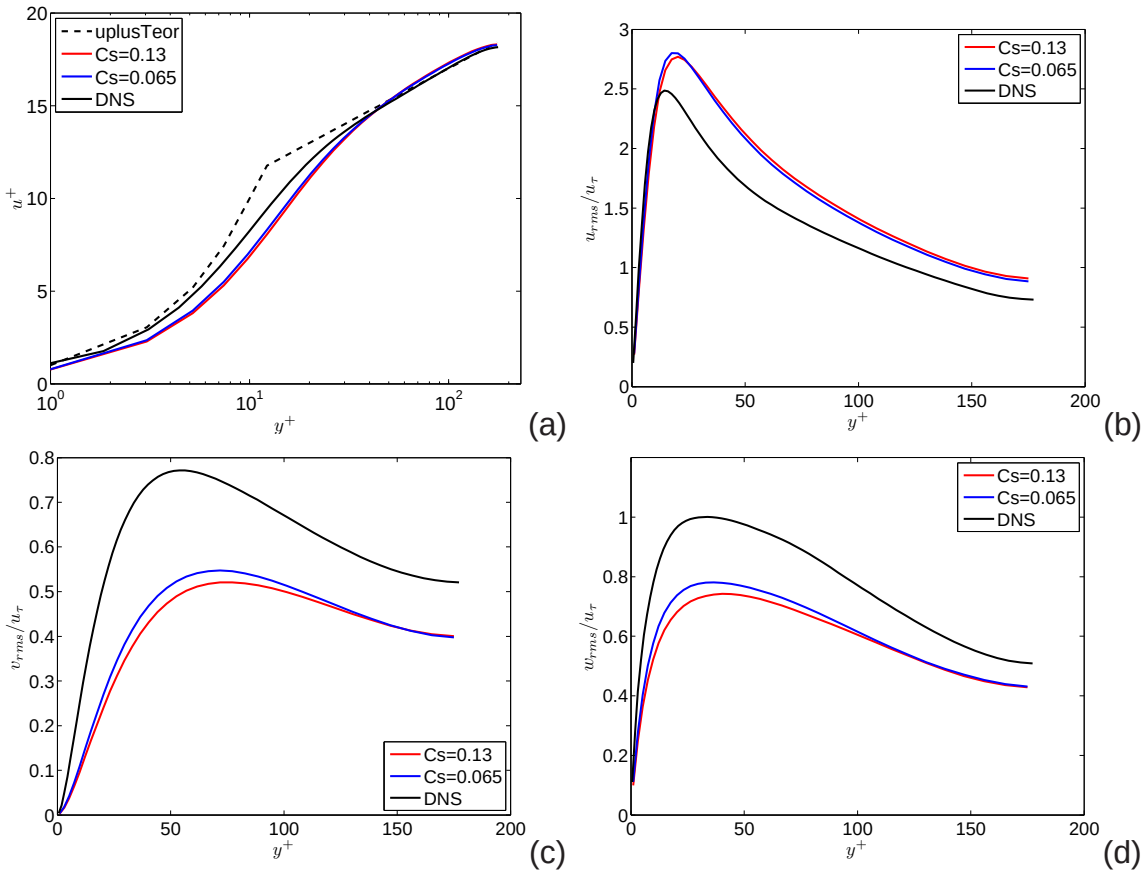

FIGURE 2.4: *Mean velocity profile (a) and rms velocity fluctuations in three directions (b-d) obtained with Vreman model with two different Smagorinsky constants.*

near to the wall and the Vreman model.The grid sizes in the streamwise and spanwise directions are set $\Delta x^+ \approx 36$ and $\Delta z^+ \approx 21$ for the wall-resolved LES simulations. Simulations were performed using the same computational mesh. In order to examine influence of models, complementary simulations were performed without an eddy-viscosity. These simulations are referred as the laminar case.

In Fig. 2.5 an instantaneous contour plot of the velocity magnitude obtained using the Vreman model is presented. We can observe, as expected, elongated and more smooth structures that develop in this flow with comparison to a similar picture obtained from DNS (Fig. 2.1). In Fig. 2.6(a-d) the mean velocity profile and rms velocity fluctuations normalized by the shear velocity, u_τ equals to 2.10^{-5}m/s are presented for a number of previously described cases. For the mean velocity, in the viscous and buffer layers, LES results significantly vary from those obtained using DNS. For the mean flow, no significant difference is found between LES results and the laminar case. From these results, it may be concluded that the significant part of dissipation in the simulations is supplied by the numerics instead of the subgrid scale eddy-viscosity modeling. For the streamwise component of the velocity, the LES results are over-predicted about 10% in comparison to DNS result. In previous section we concluded that the Vreman model has a small sensitivity to the model parameter. It can be seen as an advantage over the Smagorinsky model, which is very sensitive with respect to the C_s constant. In addition, the Smagorinsky model supplies the most under-predicted values of the rms velocity comparing to the Vreman model and the laminar case. Probably, this under-prediction is due to the application of the Van Driest damping function, which modifies eddy-viscosity in the near wall region. Similarly as for the mean velocity values, limited influence of the models was observed in comparison to the laminar case simulated without any model. In the next section, the Vreman subgrid model will be analyzed in more detail with results obtained on various meshes.

2.4 Vreman Model Simulations on Various Meshes

In this section, the LES results obtained with the Vreman model on various computational meshes are presented. Number of grid points are chosen to be the

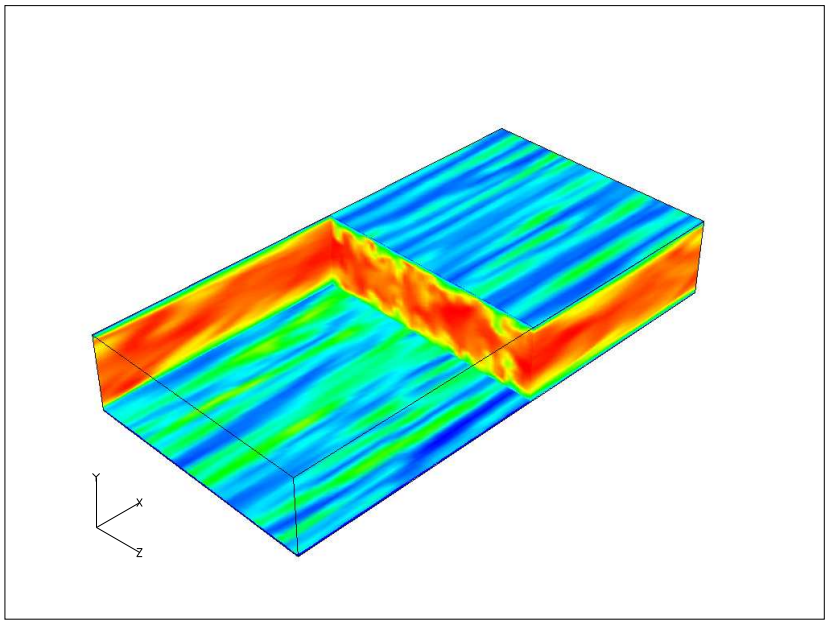

FIGURE 2.5: *Instantaneous snapshot of the velocity magnitude obtained with the Vreman model.*

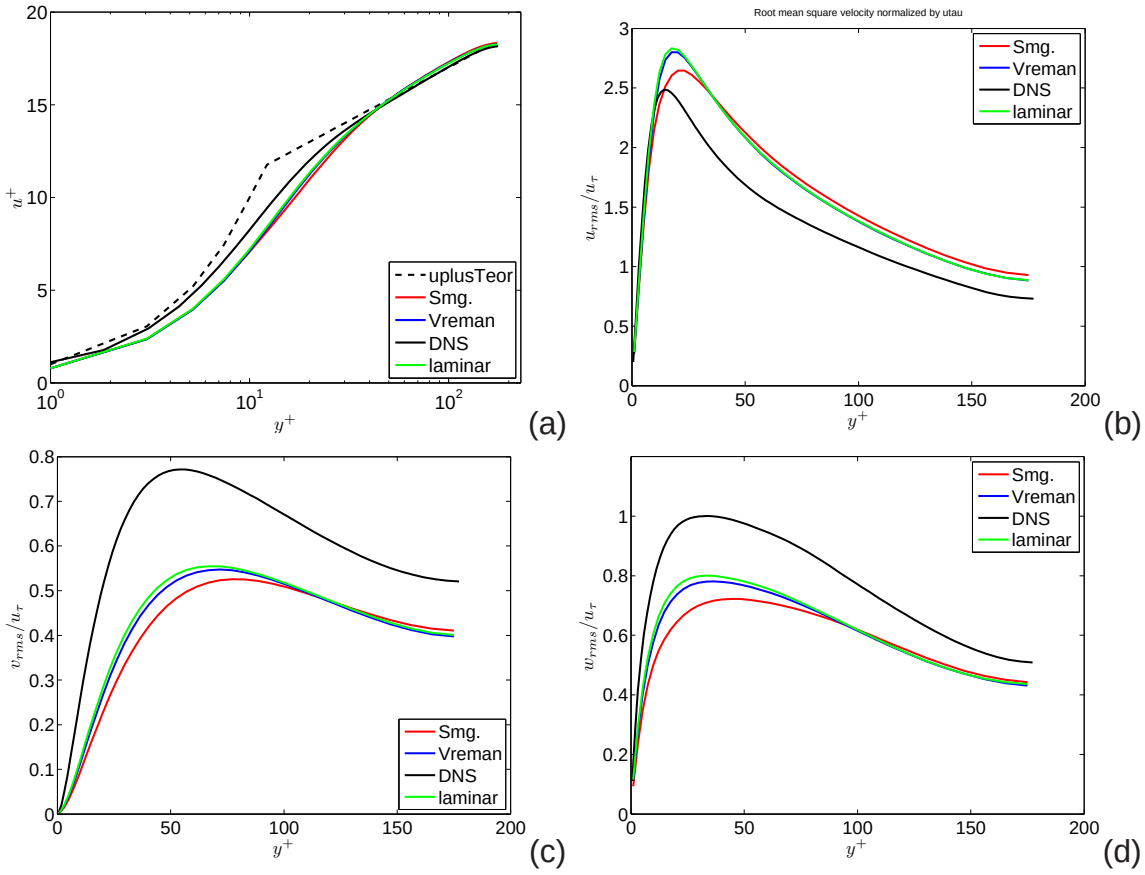

FIGURE 2.6: *Mean velocity profile (a) and rms velocity fluctuations in three directions (b-d) obtained for various models with* $C_s = 0.065$.

TABLE 2.1: *Mesh description for various wall distances*

	N_x	N_y	N_z	g_H	Total grid
$1y^+$	63	72	54	5	244944
$2y^+$	63	36	54	5	122472
$4y^+$	63	18	54	5	61236
$8y^+$	63	22	54	1	74844

same for all y^+values along the x- and z-directions, but along the y-axis the number of grid point N_y, is chosen different for each y^+. The grid sizes in the streamwise and spanwise directions are set to $\Delta x^+ \approx 36$ and $\Delta z^+ \approx 21$ for the LES simulations.

In Table 2.1 the number of grid points for each direction, growing factor g_H (defined as the ratio of last cell size in the bulk to first cell size near to the wall), and total grid size for meshes with the following typical wall distances: $1y^+$, $2y^+$, $4y^+$, $8y^+$ are presented.

These meshes were constructed to preserve the growing size of the computational cells in the normal wall direction while keeping the other discretization in the x and z directions constant. This choice was dictated by a practical approach in which the wall distance dictates the smallest size of the computational cells in the y-direction. It must be noted that in this case not only the wall distance is influenced, but also the discretization, which is particularly important in the buffer region. Simulations were performed for a sequence of wall distances from one to eight y^+ values. The low-Reynolds flow is simulated at friction Reynolds number of $Re_\tau = u_\tau \delta/\nu = 180$. The bulk mean velocity U_m for $Re_m = U_m 2\delta/\nu = 5600$ is $3.11 \cdot 10^{-4}$m/s. Assuming the current length of the domain is $L = 4\pi\delta$, one cycle time takes more than $35 \cdot 10^4$s. It was observed that the flow is developed after 12000 iterations. $30 \cdot 10^6$s flow time has been used for the development of the flow, which corresponds to 86 cycle. The collection of data is performed for 8000 iterations. $20 \cdot 10^6$s flow time has been used for the collection of the data, which corresponds to 57 cycle. 'PISO' is used as the pressure-velocity coupling method and time step, Δt is set to 2500s. The solver tolerance is set to 10^{-5} as a convergence parameter.

The mean velocity profile and rms velocity fluctuations normalized by the shear velocity, u_τ equals to $2 \cdot 10^{-5}$m/s are presented in Fig. 2.7(a-d). For the mean veloc-

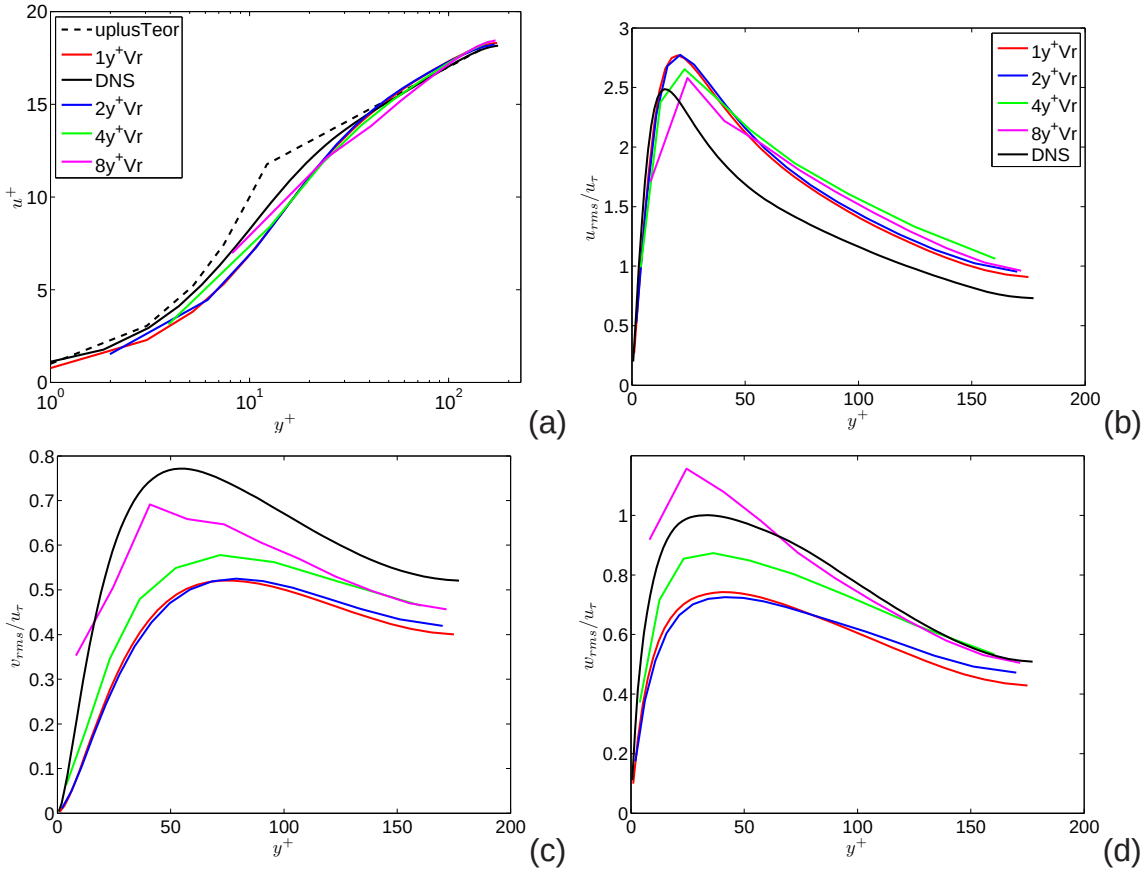

FIGURE 2.7: *Mean velocity profile (a) and rms velocity fluctuations in three directions (b-d) obtained for the Vreman model on various meshes.*

ity [Fig. 2.7(a)], large differences can be observed in the buffer region as expected. For the streamwise rms velocity component [Fig. 2.7(b)], in the viscous sublayer ($y^+ < 5$), no significant differences are observed between results obtained on various meshes. As in this region the velocity follows the linear profile, i.e., $u^+ = y^+$, these results are expected to be similar. A change in the wall distance in this region does not affect accuracy of the obtained results. Large differences in predictions of the rms velocities appear in the buffer and log layers. This is particularly visible when the results obtained on the coarsest mesh were investigated. In the next chapter we examine these differences in more detail performing simulations on the same set of the meshes changing only the wall distances.

TABLE 2.2: *Parameters used for $k-\epsilon$ model channel geometry*

$4\pi\delta(streamwise\ \ length)$	$3.52m$
$2\delta(total\ \ height)$	$0.56m$

2.5 Comparison of LES and $k-\epsilon$ Models

In this section, $k-\epsilon$ results obtained with Fluent and LES results obtained with OpenFoam are compared and presented. The channel flow was simulated at the friction Reynolds number of $Re_\tau = 180$. The bulk mean velocity U_m for $Re_m = U_m 2\delta/\nu = 5600$ is 0.01 m/s. The computational domain is chosen to be $4\pi\delta$ in the streamwise (x) direction. The height of the channel is denoted by δ in (y) direction. The computation is carried out with 1600 computational grid points. The computational domain is discretized with $40x40$ points in x and y directions. The first computational point from the wall is at $y^+ = 2$. In Table 2.2 parameters used for $k-\epsilon$ model channel geometry are presented. Velocity inlet and pressure outlet boundary conditions are used for the $k-\epsilon$ model simulation. Simulation is carried out with standard $k-\epsilon$ model and enhanced wall treatment is used as near wall treatment.

The standard $k-\epsilon$ model is a semi-empirical model based on model transport equations for the turbulence kinetic energy (k) and its dissipation rate (ϵ). In the derivation of the $k-\epsilon$ model, the assumption is that the flow is fully turbulent, and the effects of molecular viscosity are negligible. The standard $k-\epsilon$ model is therefore valid only for fully turbulent flows. The details of the model is available in Ref.[15].

In FLUENT s near-wall model, the viscosity-affected near-wall region is completely re-solved all the way to the viscous sublayer Ref.[15]. 'SIMPLE' (Semi-Implicit Method for Pressure-Linked Equations) is used as pressure-velocity coupling method, which is the numerical procedure to solve the Navier Stokes equation for steady flows.

The mean velocity profiles normalized by the wall shear velocity, u_τ equals to $6.43 \cdot 10^{-4}$m/s are presented for $k-\epsilon$ model and LES simulations in Fig. 2.8. Mean velocity profile of $k-\epsilon$ model is close to DNS. $k-\epsilon$ model's velocity profile is different from the profile of LES. The main reason of this difference is dissimilarity of the channel geometry and velocity of two turbulence models.

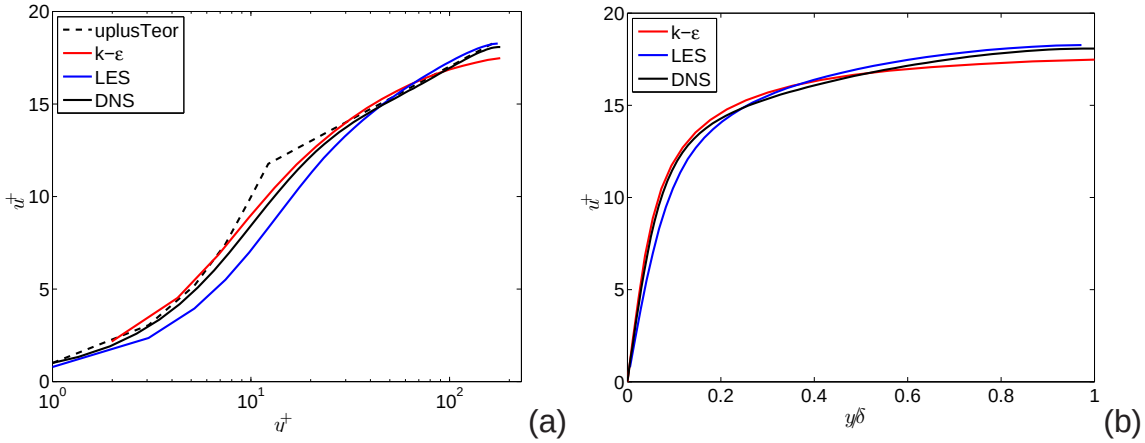

FIGURE 2.8: *Mean velocity profile in wall units (a) and in global coordinates (b) obtained with $k-\epsilon$ model.*

2.6 Conclusions

In this chapter, a preliminary study of numerics and LES modeling was performed for the channel flow simulations at low Reynolds number. It was shown that OpenFoam DNS delivers similar results to those obtained in the literature. LES Smagorinsky simulations give better results when the C_s constant is particularly adjusted for a channel flow ($C_s = 0.065$). With respect to that, the Vreman model gives much better results without being influenced by the value of the constant parameter. Such model behavior is expected and needed in simulations of more complicated flows. It was found that main source of the dissipation comes from the numerical schemes used in simulations instead of the SGS modeling as can be anticipated from the application of these models. In the next chapter LES is examined in more detail by performing simulations for higher Reynolds numbers.

3 CHANNEL FLOW AT HIGH REYNOLDS NUMBER

In this chapter, a flow at higher Reynolds number is examined. The geometry and conditions used for the channel flow with higher Reynolds number are based on the DNS simulation [Database of Wall Turbulence and Heat Transfer (Poiseuille channel flow)] performed by Kawamura [12]. The details of the reference case were mentioned in Section 1.6.2. LES results obtained using OpenFoam are compared with available DNS data [12].

LES is performed with the Reynolds number for the flow based on the bulk mean velocity U_m is $Re_m = 24428$. The friction Reynolds number based on the wall shear velocity u_τ is $Re_\tau = 640$. By increasing the channel half width δ and keeping the flow conditions the same as for the low-Reynolds number simulation, the friction Reynolds number is set to the required value. The computational domain is chosen to be 12.8δ and 6.4δ in the streamwise (x) and spanwise (z) directions. The height of the channel is denoted by 2δ. The grid sizes in the streamwise and spanwise directions are set $\Delta x^+ = 44$ and $\Delta z^+ = 26$. In the y-direction the distance from the wall is 1y^+. Simulation is carried out with 4256000 ($224 \times 100 \times 190$) grid points. 'PISO' is used as pressure-velocity coupling method and time step, Δt is set to 2500s. The solver tolerance is set to 10^{-5} as a convergence parameter. In the following sections, the wall-resolved LES simulations are performed.

The following issues are analyzed:

- investigation of the influence of LES subgrid scale models on results with comparison to DNS,
- investigation of the influence of spatial discretization in x- and z-directions on the LES results,
- testing application of wall functions at various wall distances: $1y^+$, $8y^+$, $16y^+$, $36y^+$ and $64y^+$

An instantaneous snapshot of the velocity magnitude from this simulation is presented in Fig. 3.1.

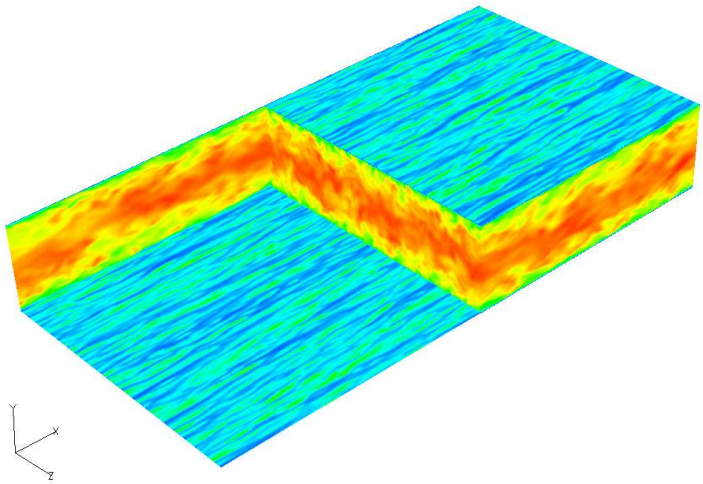

FIGURE 3.1: *Instantaneous snapshot of the velocity magnitude from the OpenFoam LES simulation at higher Reynolds number.*

3.1 SGS Model Strength and Comparison of LES Results with DNS Results

In this section, the results obtained with two eddy-viscosity subgrid models are compared. These are the Smagorinsky model with additional Van Driest damping near to the wall and Vreman model. Simulations were performed using the same computational mesh. In both SGS models, the Smagorinsky constant C_s was set to 0.065. In order to examine influence of models, complementary simulations were performed without eddy-viscosity. Similarly as in the previous chapter, these simulations are referred as the laminar case. Additionally, results obtained with OpenFoam LES are compared with DNS results.

The mean and root mean square (rms) velocity profiles are normalized by the wall shear velocity. The wall shear velocity u_τ was obtained from the simulations by averaging the instantaneous values obtained on both walls. The values of u_τ used in each simulation are listed in Table 3.1.

Fig. 3.2 presents the velocity profiles. As seen from the Fig. 3.2(a-d), in the buffer and log layers, LES results are significantly different from DNS results. For the mean flow [Fig. 3.2(a)], no significant difference is found between LES results and the laminar case. From these results, it may be concluded that significant part of dissipation in the simulations is supplied by the numerics instead of the subgrid

TABLE 3.1: *Average shear velocities, u_τ for the Smagorinsky SGS Model, Vreman SGS Model, laminar and DNS cases.*

$Smagorinsky\ \ SGS\ \ model$	$1.5648 \cdot 10^{-5} m/s$
$Vreman\ \ SGS\ \ model$	$1.5567 \cdot 10^{-5} m/s$
$laminar\ \ case$	$1.5689 \cdot 10^{-5} m/s$
DNS	$1.6297 \cdot 10^{-5} m/s$

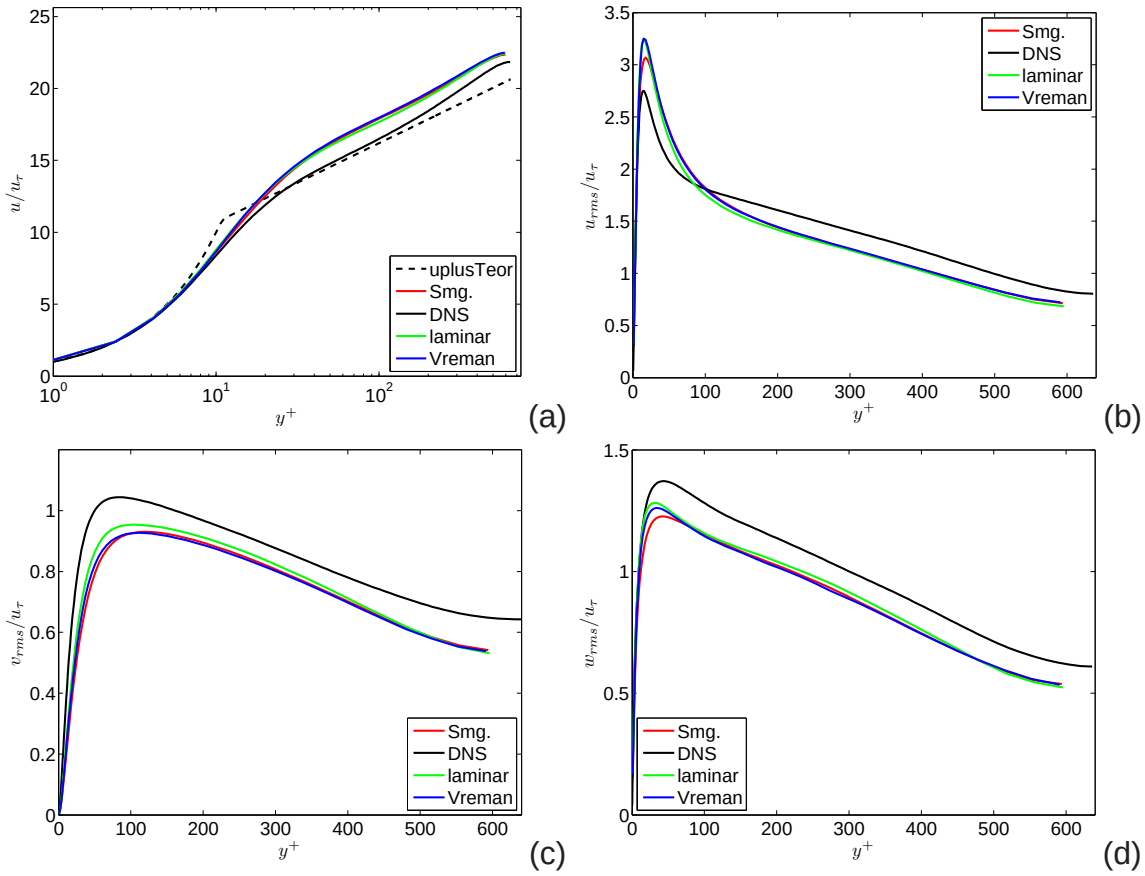

FIGURE 3.2: *Velocity profiles obtained with two SGS models (Smagorinsky and Vreman) and without model, normalized by averaged u_τ obtained from simulations: (a) mean velocity profile, (b-d) rms of velocity fluctuations in three directions. The logarithmic law of the wall denoted by dashed line.*

scale eddy-viscosity modeling. For the streamwise component of the rms velocity [Fig. 3.2(b)], the LES results are over-predicted in comparison to DNS result.

Similarly as in the previous chapter, the Smagorinsky model supplies the most under-predicted values for the rms velocities comparing to the Vreman model and the laminar case. This under-prediction supplied by Smagorinsky model is slightly less for higher Reynolds number compared to previous chapter's results. For the rms velocities in Fig. 3.2(b-d), no significant difference is found between LES results and the laminar case. This difference is slightly less than the low Reynolds number simulation results. From both the low and higher Reynolds number simulations it may be concluded that the subgrid scale eddy-viscosity model has no significant influence on the LES results. Therefore, in the next section LES is performed without using any LES subgrid model.

3.2 Influence of the Spatial Discretization

In this section the influence of different spatial discretization in the x- and z-directions is analyzed. To test the effect of spatial discretization on results, the number of cells in $x-$ and $z-$ directions were increased and decreased by a factor of 1.25. Three different set of meshes were used. The first set of mesh has $224 \times 100 \times 190$ grid points in streamwise, normal and spanwise directions resulting in 4256000 grid points. This mesh is referred as *medium* mesh and it is taken as reference in creation of two meshes. Second set of mesh, referred as a *fine* mesh was created by increasing the number of cells of the medium mesh by a factor of 1.25 in $x-$ and $z-$ directions. Third set of mesh, referred as *coarse* mesh was created by decreasing the number of cells of the medium mesh by a factor of 1.25 in $x-$ and $z-$ directions. Number of grid points are chosen to be the same for all large-eddy simulations along the y-axis. Assuming the current length of the domain is $L = 4\pi\delta$, one cycle time takes more than $1.5 \cdot 10^6$s. After 7800 iterations the flow is developed. $\approx 20 \cdot 10^6$s flow time has been used for the development of the flow, which corresponds to 13 cycle. The averaging is performed for 5675 iterations to collect the data. $\approx 14 \cdot 10^6$s flow time has been used for the collection of the data, which corresponds to 9 cycle. In Table 3.2 the grid sizes in the streamwise Δx^+ and

TABLE 3.2: *Mesh description for different cases*

	N_x	N_y	N_z	g_H	Δx^+	Δz^+	Total grid
$Medium$	224	100	190	26	44	26	4256000
$Fine$	280	100	237	26	≈ 35	≈ 21	6636000
$Coarse$	179	100	152	26	55	≈ 33	2720800

TABLE 3.3: *Average shear velocities, u_τ for the fine, medium, coarse and DNS cases.*

$Fine\ \ case$	$1.5919 \cdot 10^{-5} m/s$
$Medium\ \ case$	$1.5689 \cdot 10^{-5} m/s$
$Coarse\ \ case$	$1.5372 \cdot 10^{-5} m/s$
DNS	$1.6297 \cdot 10^{-5} m/s$

spanwise directions Δz^+, the number of grid points for each direction, growing factor g_H and total grid size are presented. In Table 3.2 the mesh descriptions are shown.

Velocity profiles are plotted in Fig. 3.3. The mean and root mean square (rms) velocity profiles are normalized by the wall shear velocity. The wall shear velocity obtained from the simulations by averaging the instantaneous values obtained on both walls. For each simulation the values of u_τ are listed in Table 3.3.

For the mean velocity in Fig. 3.3(a), in buffer and log layers significant differences were observed. As expected, the result obtained with the fine mesh is closer to DNS result than results obtained on medium and coarse meshes.

3.3 Application of Wall Functions at Various Wall Distances

In this section LES simulations are performed with various wall distances: $1y^+$, $8y^+$, $16y^+$, $36y^+$, $64y^+$. The number of grid points is chosen to be same for all simulations along the x and z directions, which are $\Delta x^+ = 44$ and $\Delta z^+ = 26$, respectively.

Computational mesh of $1y^+$ was chosen as reference while creating meshes for the other wall distances. The computational meshes were created by removing grid points close to the wall and the rest of the mesh in y-direction remained same, while

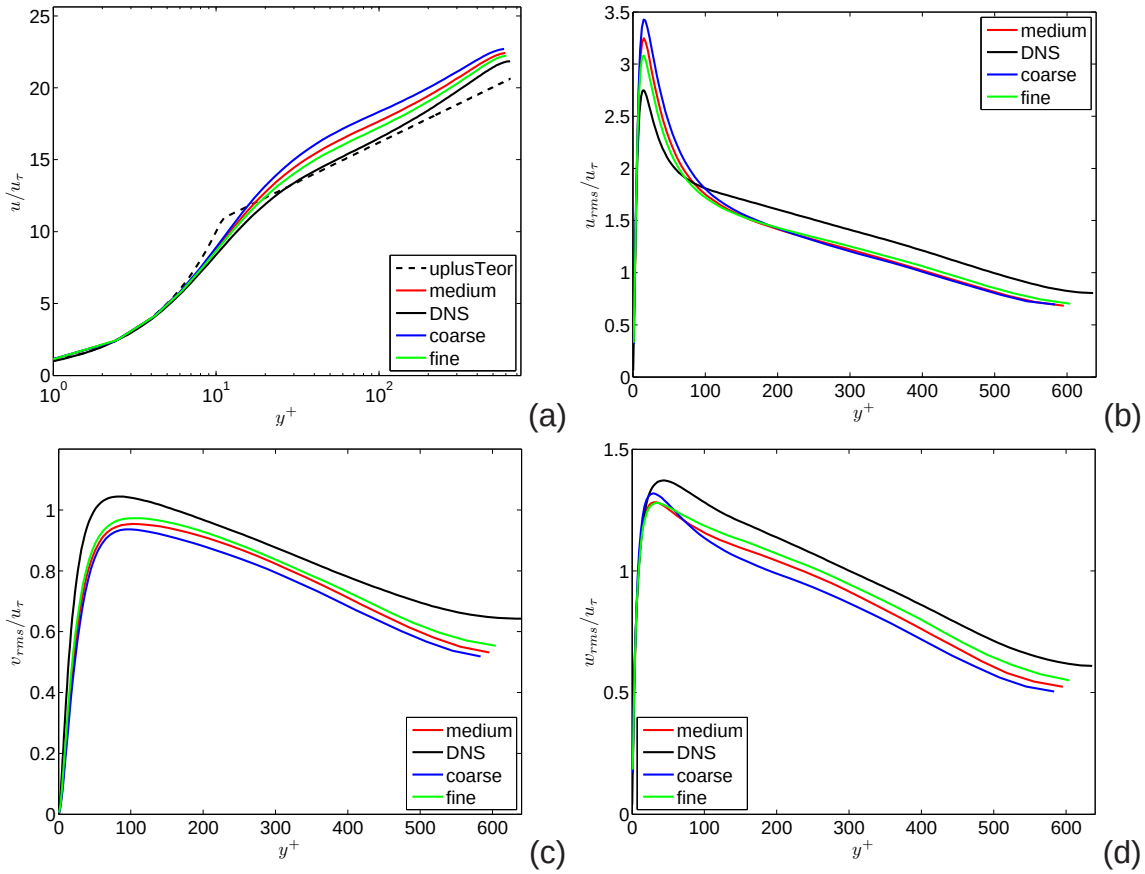

FIGURE 3.3: *Velocity profiles of fine, medium and coarse meshes normalized by averaged u_τ obtained from simulations: (a) mean velocity profile, (b-d) rms of velocity fluctuations in three directions.*

TABLE 3.4: *Average shear velocities, u_τ for various wall distances.*

$1y^+$	$1.5567 \cdot 10^{-5} m/s$
$8y^+$	$1.6034 \cdot 10^{-5} m/s$
$16y^+$	$1.3270 \cdot 10^{-5} m/s$
$36y^+$	$9.7666 \cdot 10^{-6} m/s$
$64y^+$	$7.6804 \cdot 10^{-6} m/s$
DNS	$1.6297 \cdot 10^{-5} m/s$

keeping the other discretization in x- and z- directions constant. The disadvantage of this approach is that for the larger y^+ distances there is a significant increase in the cell sizes, i.e., the first cell is much larger than the other. Such situation is rather unusual since usually computational meshes stretch with growing factors. In the low Reynolds simulations growing ratio was kept constant starting from different y^+ values. The mean and root mean square (rms) velocity profiles are normalized by the wall shear velocity. The wall shear velocity, u_τ was obtained in two ways: from the simulations and from friction Reynolds number of DNS ($Re_\tau = 640$). Hence, figures will represent the velocities normalized by both u_τ.

The wall shear velocity obtained from the simulations by averaging the instantaneous values obtained on both walls. For each simulation the values of u_τ are listed in Table 3.4.

The Fig. 3.4 presents the mean velocity profile normalized by shear velocity u_τ which was calculated by the simulations. As seen from the mean velocity profile, LES results are obviously different from DNS results. The reason is that the computation of the shear velocity evaluated from shear stress. As the shear stress is computed for various wall distances, the gradient of the velocity also changes with the change in the distance from the wall. In other words, as long as the distance from the wall varies, the shear stress is modified since the gradient of the velocity is changed. Hence, when applying wall functions the change of the shear stress caused large changes in the normalization factor (wall shear velocity) for various wall distances. As a result, the simulation results are not presented in correctly as observed in the mean profile.

In Fig. 3.5 velocity profiles normalized by the same constant u_τ, which is equal

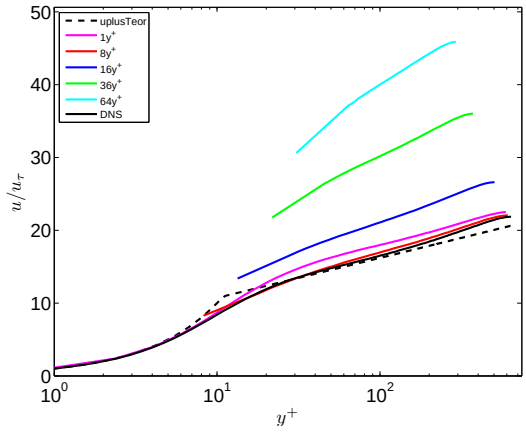

FIGURE 3.4: *Mean velocity profiles for various wall distances normalized by averaged u_τ obtained from simulations.*

to $1.6297 \cdot 10^{-5}$m/s obtained from DNS simulations are presented. As seen from Fig. 3.5(a) the mean velocity profiles for various wall distances are in good agreement with the DNS result. It may be concluded that for the presentation purposes the normalization of the results has an important influence and it should be always taken into account with caution.

3.4 Conclusions

In this chapter, the LES results were presented for the channel flow at high Reynolds number. Similarly as in the previous chapter it was shown that the Vreman model gives much better results comparing to the Smagorinsky model. The Smagorinsky model supplies the most under-predicted values for the rms velocities comparing to the Vreman model and the laminar case. This under-prediction supplied by Smagorinsky model is slightly less for higher Reynolds number when compared to previous chapter's results. Similarly, the difference between the LES results and DNS is slightly less for high Reynolds number comparing to low Reynolds number. It was found that main source of the dissipation comes from the numerical schemes used in simulations instead of SGS modeling as is expected from application of these models. It was seen that increase of the mesh resolution gives much better results. The result obtained with the fine mesh is in a better agreement with DNS result than results obtained with medium and coarse meshes. It was also seen

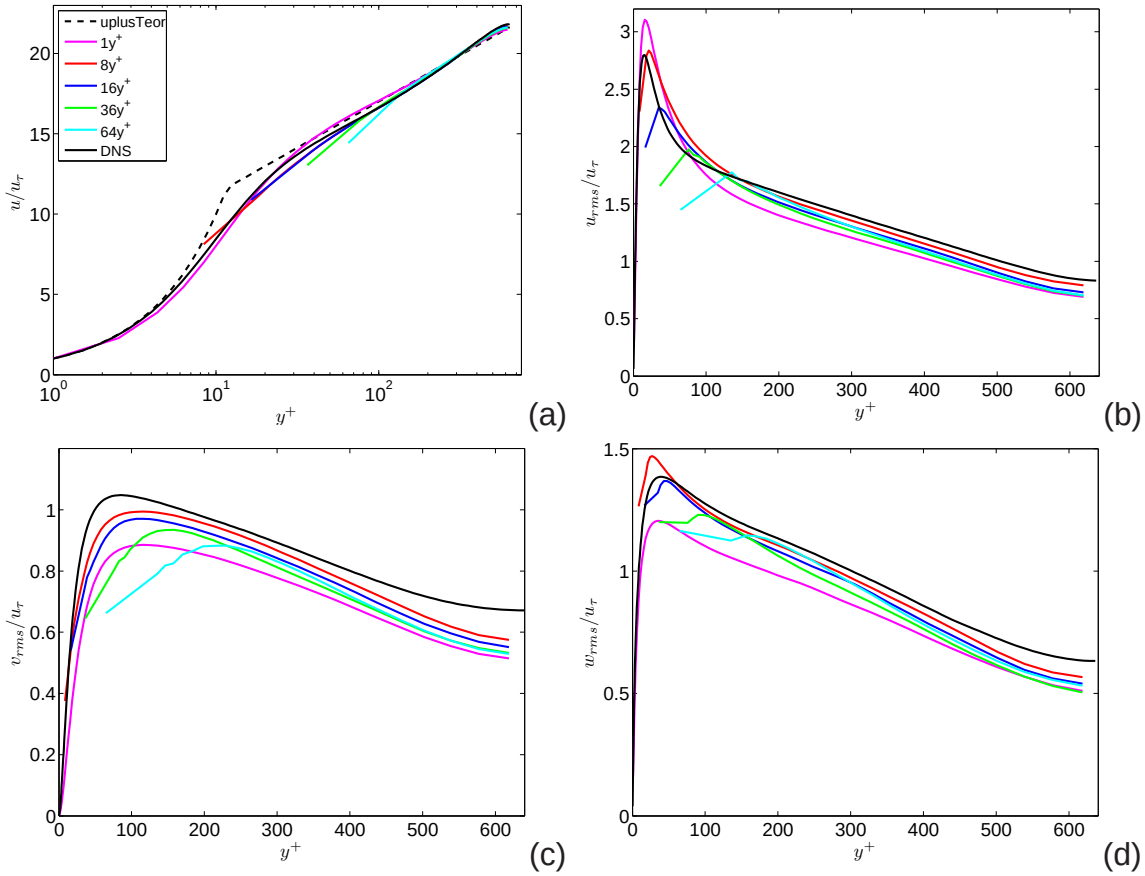

FIGURE 3.5: *Velocity profiles for various wall distances normalized by the same constant u_τ from DNS simulations: (a) mean velocity profile, (b-d) rms of velocity fluctuations in three directions.*

that the scaling has important influence in presentation of the normalized results. Mean velocity profiles for various wall distances are similar to the DNS profile.

4 LES OF TURBULENT HEAT TRANSFER

Turbulent heat transfer in a channel geometry at the friction Reynolds number $Re_\tau = 640$ and at the Prandtl number $Pr = 0.71$ is investigated in this chapter. The goal of the performed LES described in this chapter was to test implementation of the thermal wall functions for different distances from the wall: $1y^+$, $8y^+$, $16y^+$, $36y^+$, $64y^+$. The computational meshes are the same as in high Reynolds number case. The geometry and flow conditions comply with the reference DNS described in Section 1.6.2.

In this chapter LES of turbulent heat transfer is presented and the following issues are examined:

- turbulent heat transfer with the constant wall heat flux boundary condition,
- turbulent heat transfer with the constant wall temperature boundary condition,
- validation of the Jayatilleke thermal wall functions [8].

In the next subsection, LES results with the constant wall heat flux boundary condition will be presented.

4.1 Turbulent Heat Transfer with the Constant Wall Heat Flux Boundary Condition

In this section, Large-Eddy Simulations results with additional temperature equation are tested for different wall distances $1y^+$, $8y^+$, $16y^+$, $36y^+$, $64y^+$. The influence of the eddy-diffusivity modeling in LES and application of wall functions are also presented. In this section LES results refer to simulations performed with the Vreman SGS model. For LES with an eddy-viscosity model and wall function, the effective diffusivity ($\alpha_{\text{eff}} = \alpha + \alpha_t = \frac{k}{\rho c_p} + \frac{\nu_{\text{Sgs}}}{Pr_t}$) is used. To get the actual heat flux through the wall the same effective diffusivity must be used in the boundary condition definition. If the thermal wall functions are not used, then the constant heat-flux boundary condition should use the effective diffusivity, which is effectively equal only to the

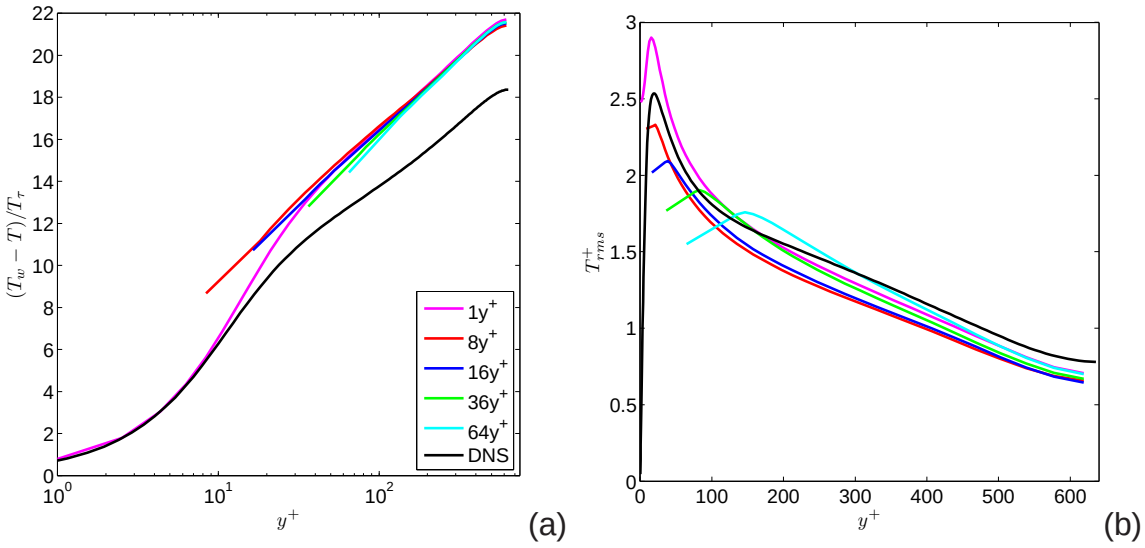

FIGURE 4.1: *Mean temperature profile (a) and rms of temperature fluctuations (b). The temperature computed without SGS model and without wall functions.*

laminar part of it ($\alpha_{\text{eff}} = \alpha = \frac{k}{\rho c_p}$). Additionally, LES is performed without any SGS model and wall functions.

Fig. 4.1(a-b) represents LES results performed without any SGS model and wall functions. The mean temperature profiles are non-dimensionalized by $T^+ = \frac{T_w - T}{T_\tau}$, where the friction temperature $T_\tau = \frac{q_w}{\rho C_p u_\tau} = 0.1512$K and the friction velocity u_τ, which is equal to $1.6297 \cdot 10^{-5}$m/s is computed from DNS. The averaged wall temperature T_w is computed from the post-processing. The root mean square temperature profiles are non-dimensionalized by T_{rms}/T_τ. It must be reminded that in case of DNS simulations described in Ref. [7], the constant temperature conditions are used and temperature fluctuations at the walls are set to zero as boundary conditions. Our LES simulations are performed with the actual constant wall-heat flux boundary conditions. As seen from Fig. 4.1(b), rms temperature of DNS at the wall is equal to zero due to application of the boundary conditions that mentioned earlier. Since the boundary conditions for LES and DNS are different, for the next simulation DNS data will not be used as reference in rms temperature. Fig. 4.2(a-b) represents the LES results performed for different distances from wall: $1y^+$ and $16y^+$. LES results that refer to these simulations were performed for two cases: $Case1$ and $Case2$. $Case1$ describes the simulations performed without SGS model and wall functions. The simulations performed with SGS model named as $Case2$ were investigated in two variants: with and without wall functions. As seen from Fig. 4.2(a), SGS model has

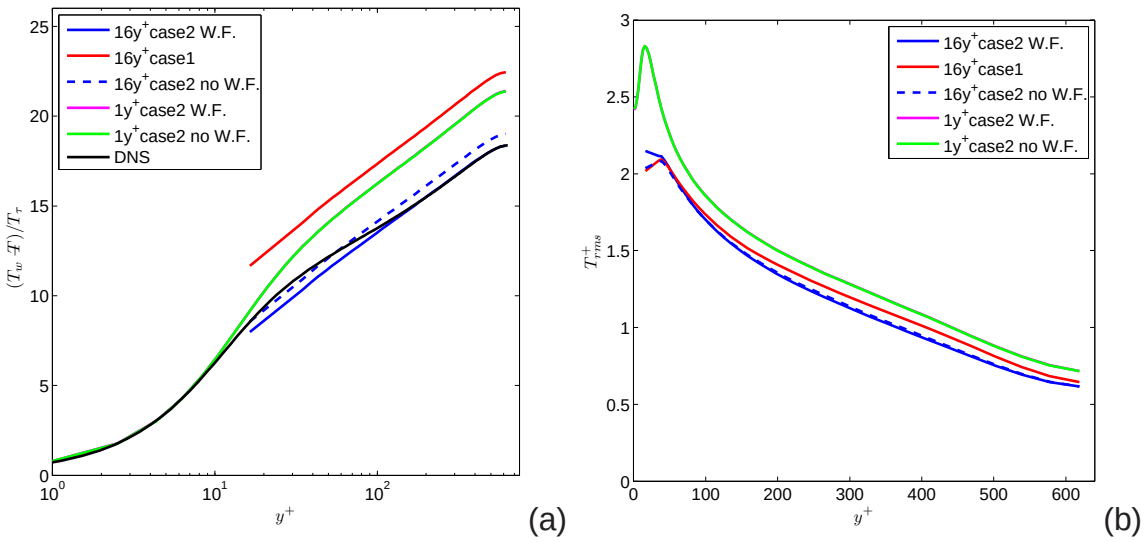

FIGURE 4.2: *Mean temperature profile (a) and rms of temperature fluctuations (b). Case1: no WF and no SGS model, Case2: with SGS model.*

large influence on the mean profile. Similarly in Fig. 4.2(b), the significant differences are observed in simulations performed with and without SGS model. Dissipative behavior of LES scheme in the OpenFoam was supplied by the numerics instead of the model as seen earlier for the momentum (velocity). In addition, it is also shown that application of the thermal wall-functions improves numerical results mainly in the bulk flow as the results close to the buffer zone cannot be reproduced without proper selection of the wall-generated turbulence for the given Prandtl number.

In the next section, LES results with the constant wall temperature boundary condition will be presented.

4.2 Turbulent Heat Transfer with the Constant Wall Temperature Boundary Condition

In this section, the large-eddy simulation results for the constant wall temperature boundary condition are presented. In our computational setup, the temperature of the walls was set to 300K. The LES simulations are performed with and without wall functions for $16y^+$. Fig. 4.3(a-b) represent LES results. The mean temperature profiles are non-dimensionalized by $T^+ = \frac{T_w - T}{T_\tau}$, where the friction temperature $T_\tau = \frac{q_w}{\rho C_p u_\tau}$ is computed from q_w and u_τ. The averaged wall heat flux q_w is computed

TABLE 4.1: *Computed average wall heat flux q_w and friction temperature T_τ for the constant wall temperature boundary condition.*

$q_w \ for \ W.F$	$5.4545 W/m^2$
$q_w \ for \ no \ W.F$	$5.2462 W/m^2$
$T_\tau \ for \ W.F$	$0.0825 K$
$T_\tau \ for \ no \ W.F$	$0.0793 K$

from the post-processing. The friction velocity u_τ is computed from DNS, which is equal to $1.6297 \cdot 10^{-5}$m/s.

The computed average wall heat flux q_w and friction temperature T_τ are shown in Table 4.1 for the simulations performed with and without wall functions.

In case of DNS simulations described in Ref. [7], the constant temperature conditions are used and temperature fluctuations at the walls are set to zero as boundary conditions.

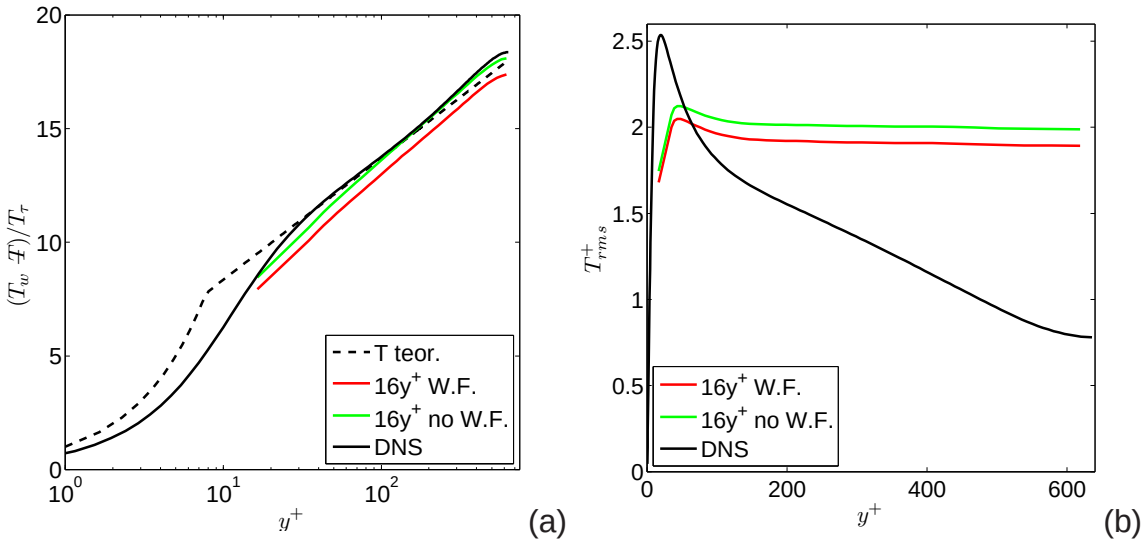

FIGURE 4.3: *Mean temperature profile (a) and rms of temperature fluctuations (b). The temperature computed with and without wall functions.*

For these conditions the quasi steady-state conditions were not obtained in a given time-framework. This is probably due to larger time needed for the thermal conditions to develop or due to errors in boundary or forcing conditions implementation. Due to this fact, the averaged q_w needed for the normalization is still changing within the averaged period. As a result, the mean profiles are rather is questionable

when compared to the DNS results. In addition, rms profiles exhibit flat behavior in the simulation results for the bulk of the flow. Further studies should be devoted for the application of this approach. These were not feasible due to time limitations in the current project.

4.3 Conclusions

In this chapter, turbulent heat transfer in a channel geometry at $Re_\tau = 640$ and $Pr = 0.71$ was investigated. LES was performed for the constant wall heat flux and wall temperature boundary conditions. The influence of SGS model and thermal wall functions were tested. It was found that SGS model has large influence on the mean temperature profile. Similarly, wall functions have an impact on the mean and rms fluctuations. It was observed that the results are much more sensitive to the scaling with respect to averaged values obtained from the simulations in the developed conditions. More simulation time is needed to compute proper T_w for the constant heat flux and q_w for the constant temperature boundary conditions. Code and implementation must be revised in order to examine the non-quasi-steady conditions coming from the application of the constant wall temperature boundary conditions.

5 SUMMARY AND CONCLUDING REMARKS

The main goal of the thesis was to test the application of wall functions applied to LES for turbulent channel flow. The concerning simulations were performed using OpenFoam CFD code. Several important results have been observed. Primarily, it was necessary to obtain the appropriate LES flow conditions that must be used in a channel flow. For this reason firstly, the flow conditions were tested at low Reynolds number as presented in Chapter 2. Additionally in the second chapter, DNS were performed to check the accuracy of the OpenFoam numerical scheme. It was shown that the OpenFoam DNS results delivered similar results comparing to the available test-case DNS data. Based on this, OpenFoam DNS was taken as a reference case for further analysis. One of the important results was the influence of subgrid scale constant. LES Smagorinsky simulations gave better results when the constant was particularly adjusted for a channel flow. With respect to that, the Vreman model gave much better results without being influenced by the value of the constant parameter. The Smagorinsky and Vreman eddy-viscosity subgrid models were compared and the Smagorinsky model gave the most under-predicted values for the rms velocities comparing to the Vreman model. Probably, this under-prediction comes from the application of the Van Driest damping function, which modifies eddy-viscosity in near wall region.

The analysis presented in Chapter 2 showed that change in the wall distance caused large differences in predictions of the rms velocities that appeared in the buffer and log layers. This was particularly visible when the results obtained with the coarsest mesh scheme was investigated.

In Chapters 2 and 3 the influence of SGS model was investigated. It was shown that the subgrid scale eddy-viscosity model had no significant influence on the LES results. It was found that the main source of the dissipation comes from the numerical schemes used in simulations instead of the SGS modeling.

In Chapter 3, it was shown that increasing the mesh resolution by changing the spatial discretization in the streamwise and spanwise directions gave much better results. The result obtained with the higher resolution mesh was in better agreement with the DNS result than results obtained with the lower resolution meshes.

In Chapter 4, the analysis performed for the turbulent heat transfer at high Reynolds number was presented for the constant wall heat flux and wall temperature boundary conditions. Modeling had large influence on the mean temperature profile. From the testing of application of thermal wall functions it was found that wall functions had an impact on the mean and rms fluctuations. It was observed that the results are much more sensitive to the scaling with respect to averaged values obtained from the simulations in the developed conditions. More simulation time is needed to compute proper T_w for the constant heat flux and q_w for the constant temperature boundary conditions.

The main concern of the thesis was implementation of wall functions to LES. If the goal is to predict the flow in a bulk, then wall functions can be used for the conditions that they were developed for. Since the channel flow is wall generated turbulence, the maximum temperature or velocity fluctuations are close to the wall. The wall functions fail to predict these values if they are used for usual RANS distance equal to 30:100 y^+. If the fluctuations close to the wall are needed to be predicted, wall functions shouldn't be used.

5.1 Future Work

Testing the application of wall functions, which is the main purpose of this work can be done in less demanding and more realistic configurations (e.g., mixing-T). When mixing-T is compared to the channel geometry, it is more difficult. The flow conditions can be less controlled. However, it is probably a less demanding case due to turbulence is generated in the bulk by mixing layers and flow that hits the wall.

Another suggestion related to this work is to compute heat-flux correctly and to check normalization factors.

OpenFoam code formulation and implementation must be revised in order to examine not quasi-steady conditions coming from the application of the constant wall temperature boundary conditions.

REFERENCES

[1] J. M. McDonough. *Introductory Lectures on Turbulence*. Departments of Mechanical Engineering and Mathematics University of Kentucky, 2004, 2007.

[2] B. E. Launder and D. B. Spalding. *Mathematical Models of Turbulence*. Academic Press, 1972.

[3] J. W. Deardorff. A numerical study of three-dimensional turbulent channel flow at large Reynolds numbers. *J. Fluid Mech.*, 41:453, 1970.

[4] J. H. Ferziger. Large-eddy and direct simulation of turbulnet flows. in lecture notes for the short course on calculations of turbulent flows. Technical report, University of Hamburg, 1995.

[5] A. W. Vreman. An eddy-viscosity subgrid-scale model for turbulent shear flow: algebraic theory and applications. *Physics of Fluids*, 16(10):3670–3681, 2004.

[6] S. B. Pope. *Turbulent flows*. Cambridge University Press, 2000.

[7] H. Kawamura, K. Ohsaka, H. Abe, and K. Yamamoto. DNS of turbulent heat transfer in channel flow with low to medium-high Prandtl number fluid. *International Journal of Heat and Fluid Flow*, 19:482–491, 1998.

[8] C. L. V. Jayatilleke. The influence of Prandtl number and surface roughness on the resistance of the laminar sublayer to momentum and heat transfer. *Prog. Heat Mass Transfer*, 1:193–329, 1969.

[9] W. Schoppa and F. Hussain. Coherent structure dynamics in near-wall turbulence. *Fluid Dynamics Research*, 26:119–139, 2000.

[10] Kim et al. Channel flow-DNS. Technical report, Ercoftac classic database, 1987.

[11] P. Moin J. Kim and R. Moser. Turbulence statistics in fully developed channel flow at low Reynolds number. *J. Fluid Mech.*, 177:133–166, 1987.

[12] H. Abe and H. Kawamura. Direct numerical simulation data base for turbulent channel flow with heat transfer. Technical report, Department of Mechanical Engineering Tokyo University of Science Noda-shi, Chiba 278-8510, Japan, 2004.

[13] OpenFoam, The Open Source CFD Toolbox, user guide, version 1.5, July 2008.

[14] Openfoam, The Open Source CFD Toolbox, programmmer's guide, version 1.5, July 2008.

[15] Fluent 6.3 User's Guide, September 2006.

A Appendix

TABLE A.1: *Parameters used for channel geometry*

	$Re_\tau = 180$	$Re_\tau = 640$
δ	$9m$	$39.27m$
$4\pi\delta(streamwise\ \ length)$	$113.09m$	$493.48m$
$2\pi\delta(spanwise\ \ length)$	$56.55m$	$246.74m$
$2\delta(total\ \ width)$	$18m$	$78.54m$

CURRICULUM VITAE

Name and Surname	: Ufuk Korkmaz
Place of birth	: Ankara
Date of birth	: 02.10.1982
Marital Status	: Single
Education and Academic Position	: Hacettepe University, MSc in Nuclear Engineering
High School	: 1997-2000, Cumhuriyet Lisesi, Ankara
Undergraduate	: 2001-2007, Hacettepe University, Nuclear Engineering Department
Foreign Language	: English